Acta Geologica Sinica (English Edition), 2019, 93(6): 1835–1849

Petrography and Geochemistry of the Upper Triassic Sandstones from the Western Ordos Basin, NW China: Provenance and Tectonic Implications

ZHAO Xiaochen[1], LIU Chiyang[2, *], XIAO Bo[3], ZHAO Yan[4] and CHEN Yingtao[1]

[1] *College of Geology and Environment, Xi'an University of Science and Technology, Xi'an 710054, China*
[2] *State Key Laboratory of Continental Dynamics, Department of Geology, Northwest University, Xi'an 710069, China*
[3] *Fifth Oil Production Plant of Changqing Oilfield, Xi'an 710200, China*
[4] *Chang'an University, Xi'an 710064, China*

Abstract: Petrographic and geochemical characteristics of the Upper Triassic sandstones in the western Ordos Basin were studied to provide insight into weathering characteristics, provenance, and tectonic implications. Petrographic features show that the sandstones are characterized by low-medium compositional maturity and textural maturity. The CIA and CIW values reveal weak and moderate weathering history in the source area. The geochemical characteristics together with palaeocurrent data show that the northwestern sediments were mainly derived from the Alxa Block with a typical recycled nature, while the provenance of the western and southwestern sediments were mainly from the Qinling-Qilian Orogenic Belt. The tectonic setting discrimination diagrams signify that the parent rocks of sandstones in the western and southern Ordos Basin were mainly developed from continental island arc, which is closely related to the evolution of the Qinling-Qilian Orogenic Belt. However, the sandstones in the northwestern Ordos Basin show complex features, which may be resulted from a typical recycling process. Overall evidence from petrography, geochemistry and sedimentology, together with previous researches suggest the Kongtongshan and Helanshan areas were the southwestern and northwestern boundary of the Ordos Basin, respectively, and there was no clear boundary between the Hexi Corridor Belt and Ordos Basin, where a large, uniform sediment dispersal system developed during the Late Triassic.

Key words: western Ordos Basin, upper Triassic, geochemistry, petrography, provenance analysis, proto-boundary

Citation: Zhao et al., 2019. Petrography and Geochemistry of the Upper Triassic Sandstones from the Western Ordos Basin, NW China: Provenance and Tectonic Implications. Acta Geologica Sinica (English Edition), 93(6): 1835–1849. DOI: 10.1111/1755-6724.13863

1 Introduction

The Ordos Basin is located in the western part of the North China Block (NCB) (Fig. 1a) and formed as an intracontinental basin with highly deformed and complicated basin margins (Yang et al., 1986; Liu et al., 2006; Xie, 2016). This basin is the second largest sedimentary basin in China with rich deposits of coal, oil, uranium and natural gas (Bao et al., 2014; Wang et al., 2018; Wu et al., 2018). It developed during the Middle Triassic to Early Cretaceous in a position superimposed upon the larger Palaeozoic North China Craton (Liu et al., 2006). The Ordos Basin is bounded by the Yinshan belt (Daqingshan and Langshan mountains) to the north, the Lvliang and Taihang mountains to the east, the Qinling Mountain ranges to the south, and the Liupan and Helan mountain ranges to the west (Liu et al., 2006). During the Cenozoic, a series of grabens developed between those mountains and the Ordos Basin, including the Hetao graben to the north, the Shanxi graben to the east, the Weihe graben to the south and the Yinchuan graben to the west.

The western Ordos Basin is located at the conjunction of several geo-tectonic parts with various structure features and complicate evolution processes (Fig. 1b; Liu et al., 2005; Bai et al., 2006; Zhao et al., 2006). Nowadays, most people share the opinion that the Upper Triassic Yanchang Formation in Ordos Basin performs as an important source rock (Duan, 2012; Liu et al., 2013; Wang et al., 2014; Zhao et al., 2017), making it important to determine the boundary of the western Ordos Basin during this period. Over the past decades, various discussions and researches have been done on the regional geological structural characteristics and tectonic setting/ attributes of the western Ordos Basin, different opinions have been proposed (e.g., Yang, 1990; Tang et al., 1992; Yin and Nie, 1996; Liu and Yang, 1997; Zhang, 2002; Liu et al., 2005; Zhao et al., 2006; Yang et al., 2011). In the northwestern Ordos, previous workers have proposed either foreland basin (Sun et al., 1989; Yin and Nie, 1996; Stephen and Mark, 1999) or extensional settings (Liu, 1998; Liu and Yang, 2000; Ritts et al., 2004; Wang et al., 2005; Liu et al., 2006; Yang et al., 2010). Also, some researchers considered the southwestern and northwestern margin of the Ordos Basin as a whole (Yang, 1990; Tang et al., 1992; Yin and Nie, 1996). Furthermore, some

* Corresponding author. E-mail: zxcnwu@126.com

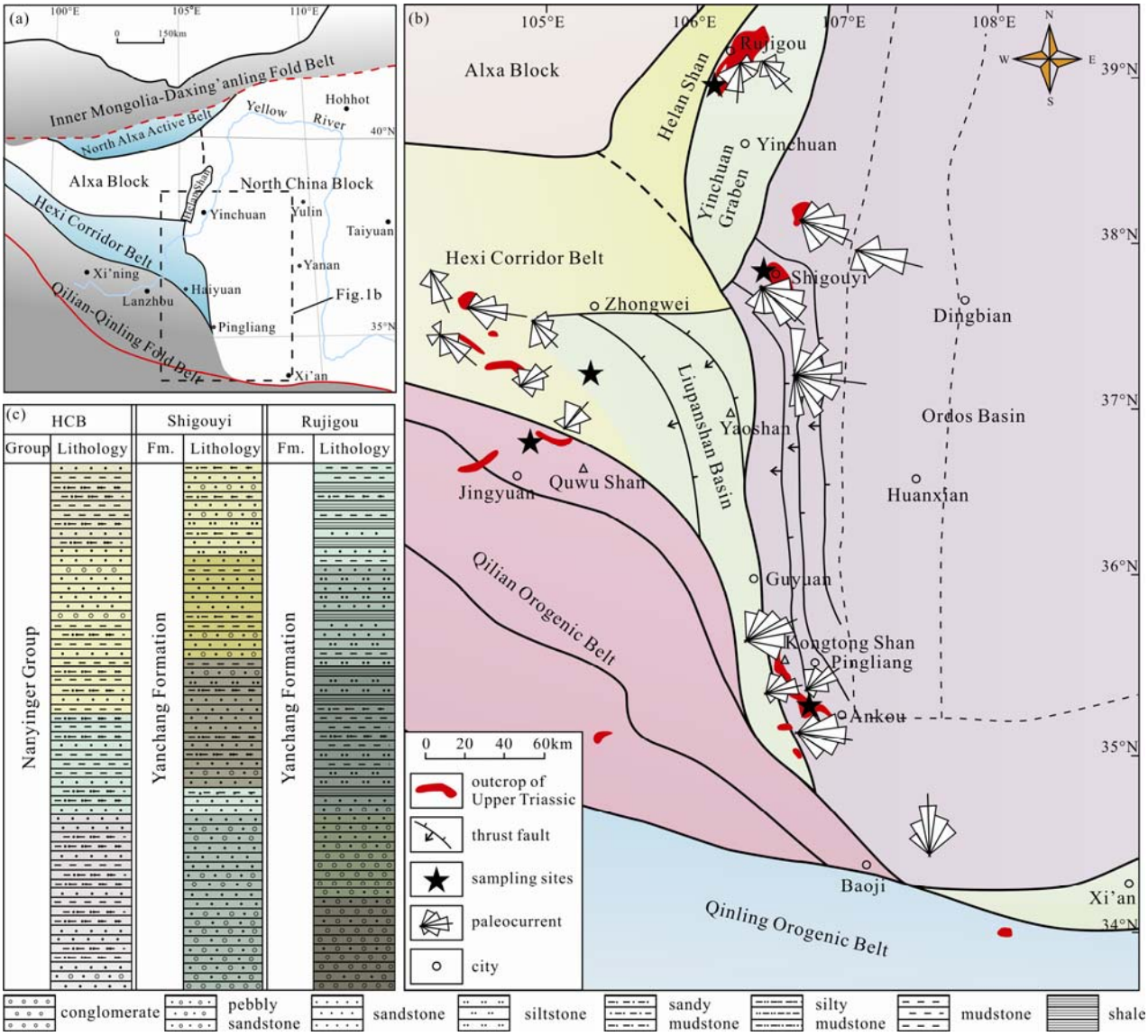

Fig. 1. (a) Tectonic sketch map of the study area; (b) simplified geological map of the western margin of the Ordos Basin, showing location of the sandstone samples and palaeocurrent (after Zhao et al., 2006); (c) stratigraphic column of the Upper Triassic strata in different sections.

researchers interpreted the idea that there were different tectonic histories and sedimentation styles in the northwestern and southwestern Ordos Basin (Liu and Yang, 1997; Liu, 1998; Liu et al., 2005; Yang et al., 2005; Liao et al., 2007; Ritts et al., 2009).

In this study, we provide petrographic and geochemical data of the Upper Triassic sediments in the western Ordos Basin. The main purpose is to analyze the diversity of provenance and tectonic implications for samples in western Ordos Basin and to discuss the boundary of the western Ordos Basin during the Late Triassic.

2 Tectonic Settings and Subunits

The western Ordos Basin is located in the northern segment of the North-South Tectonic Belt, which is situated in the conjunction region among the Ordos Block, the Alxa Block, the Qinling-Qilian Orogenic Belt and the Xing-Meng Orogenic Belt and separating the East and West China's continental tectonics (Liu et al., 2005; Zhao et al., 2016). Prior to the Permian, the tectonic history of the study area evolved as part of the NCB (Liu et al., 2006; Xie and Heller, 2013). The Triassic collision between the North and South China blocks and the Early Palaeozoic suture between the Qaidam Block and the Eurasian Block took place along the NCB margins (e.g., Waston et al., 1987; Xie and Heller, 2013; Dong and Santosh, 2016). In the Ordos Basin, the Upper Triassic Yanchang Formation is a set of inland depression lacustrine delta with open flow (Liu et al., 2012), which is divided into Chang 1 to Chang 10 oil layers from top to bottom based on lithology and depositional cycle (Li et al., 2012). And the Upper Triassic is widely distributed in the western Ordos Basin (Fig. 1b).

The western Ordos Basin is associated with four nearly E-W trending subparallel tectonic units, from north to south, they are (a) the Alxa Block, (b) eastern Hexi Corridor Belt, (c) the Qilian Orogenic Belt and (d) the Qinling Orogenic Belt.

2.1 Alxa Block

The Alxa Block is located in the northwestern Ordos Basin. Geographically, the Alxa Block is a desert-covered area with fault-bounded massifs. It consists predominantly of Early Precambrian basement with 2.3-1.9 Ga tonalitic/ granitic gneisses (Li et al., 2004a, b; Xiu et al., 2004; Geng et al., 2006) and it was overlain by Cambrian to Middle Ordovician cover sequences (BGMRNHAR, 1990). The Archean basement is signified by the ~2.7Ga amphibolites in the northeast of the Block (Geng et al., 2006), as well as by some 2.5-3.5 Ga detrital zircons from meta-sedimentary sequences (e.g., Geng et al., 2007; Tung et al., 2007a, b).

2.2 Eastern Hexi Corridor Belt

The eastern Hexi Corridor Belt (HCB) is bounded by the northerly Alxa Block and the Qilian Orogenic Belt (QOB) to the south (Fig. 1b). This tectonic belt is mainly characterized by clastic carbonate and flysch formation with a small amount of basic volcanic rocks during the Early Palaeozoic (Zhao et al., 2016). The fold and uplift processes occurred after Silurian led to the formation of depressions from Late Palaeozoic to Triassic with the strata characterized by coal-bearing clastic rocks. The Indosinian movement at the end of the Triassic resulted in strong folding and thrusting of the strata, accompanied by medium and low temperature hydrothermal activity. Under the effect of Indosinian and Yanshan movement, the HCB formed the intermountain graben with coal-bearing strata, saliferous strata and red bedded building from Jurassic to Neogene.

2.3 Qilian Orogenic Belt

The Qilian Orogenic Belt is located in a joint region among the three major blocks in China, i.e., the NCB in the northeast, the Yangtze Block in the southeast and the Tarim Block in the northwest (Song et al., 2013). This belt is a typical oceanic suture zone and contains Neoproterozoic to Early Palaeozoic ophiolite sequences, HP metamorphic belts, island-arc volcanic rocks and granitoid plutons, Silurian flysch formations, Devonian molasse, and Carboniferous to Triassic sedimentary cover sequences. The eastern Qilian Orogenic Belt that is adjacent to the basin is composed of Mesoproterozoic Longshan Group gneiss and marble, Sinian to Middle Ordovician Huluhe Group and Upper Ordovician Chenjiahe Formation metamorphic detrital rocks and meta -basic volcanic rocks, Sinian to Ordovician dolomite, sandstone and shales and Permian to Triassic clastic rocks (Liu et al., 1997).

2.4 Qinling Orogenic Belt

The Qinling Orogenic Belt is located between the North China and South China Blocks, and has been considered to have been formed by the collision between these blocks (Dong and Santosh, 2016). Beginning in the Early to Late Triassic, the Qinling Orogenic Belt formed the southern boundary of Ordos Basin (Xie and Heller, 2013). It experienced complex arc-continent and continent-continent suturing and collision during the Late Palaeozoic to Early Mesozoic (Kröner et al., 1993; Zhang et al., 1995; Bruguier et al., 1997). As a result, different source rocks, Archean to Paleoproterozoic metamorphic rocks, Late Palaeozoic and Mesozoic sedimentary and igneous rocks, have been structurally juxtaposed together (Zhang et al., 1995).

3 Sampling and Analytical Methods

A total of 24 fresh and fine-grained sandstone samples were collected for this study from outcrops located in the western Ordos Basin. Special attention was given to the samples for better stratigraphic correlation and to make sure the analytical samples are synchronous in different sections. The floras in selected sections are all belong to northern Danaeopsis-Bernoullia assemblage, which could be comparable to that of the Yanchang Formation in the Ordos Basin, suggesting they are synchronous (BGMRGP, 1989; BGMRNHAR, 1990). Furthermore, lithological associations, sequence features and isotopic chronology also indicate that all samples in different sections are synchronous (BGMRNHAR, 1990; Liu, 2009; Xin et al., 2013a). The representative Upper Triassic outcrops, from northwest to southwest, are described here.

The Yanchang Formation in Rujigou area disconformably overlies the Middle Triassic Zhifang Formation (T_2z). It consists of yellowish green conglomerate and coarse grained subarkose in the lower subsection, fine grained sandstones with interbedded black shale in the middle subsection and yellowish green, fine grained sandstone and siltstone interbedded with dark-grey siltstone and shale in the upper subsection (Figs. 1c, 2a). The outcrop anatomy records a downward-coarsening feature in Yanchang Formation. The upward transition from coarse grained sandstone to interbedded siltstone and shale is consistent with an upward-deeping trend within a fluvial and lacustrine setting. While in Shigouyi area, the Yanchang Formation is composed mainly of grey-green, grey-yellow medium to coarse feldspathic sandstone, pebbly sandstone interbedded with grey-green silty mudstone or grey-black mudstone in the lower subsection and grey-green clay conglomerate in the upper subsection (Figs. 2b, 2c). Cross bedding is widely developed in sandstone, suggesting fluvial or deltaic plain distributary channel environment. In Kongtongshan area, the Yanchang Formation is a succession of alluvial deposits that are dominantly cobble-conglomerate, interbedded with medium- to coarse-grained sandstone (Fig. 2e). To the northeast, it is a fluvial-deltaic succession that is composed of thick-bedded arkose and dark gray to black shale (Fig. 2f). The synchronous sediment in HCB is Nanying'er Group. It consists generally of grey-green or dark-grey argillaceous siltstone and silty mudstone that occurs interbedded with grey-green or yellow-grey lithic arkose sandstone, arkose and siltstone (Fig. 2d). In Baojishan area, the bottom of the Nanying'er Group is

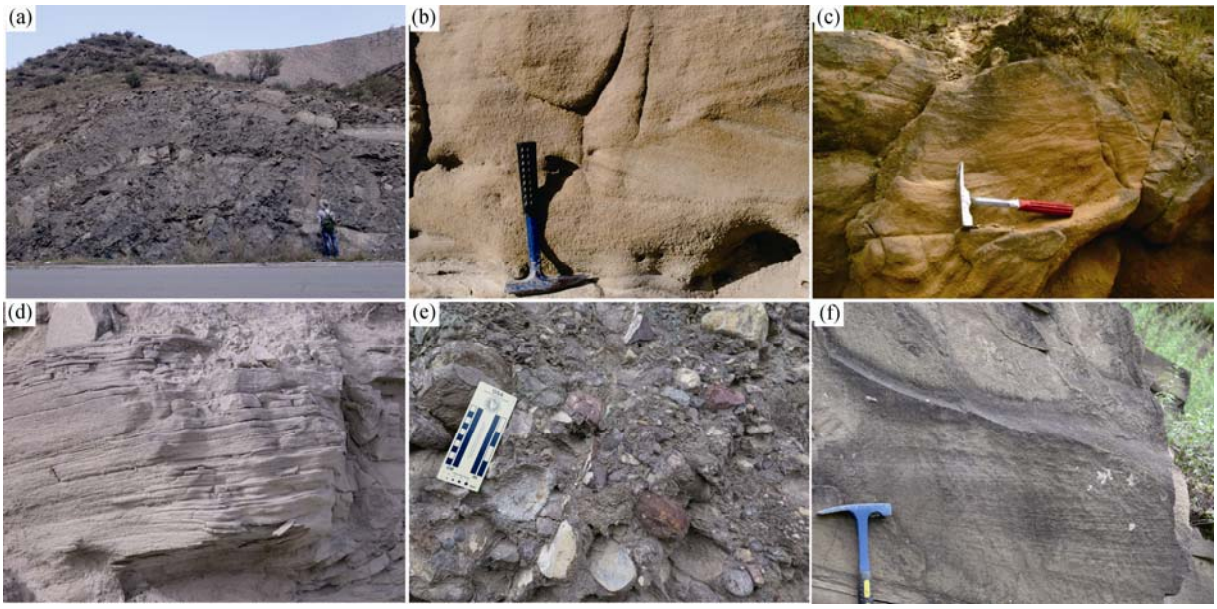

Fig. 2. Outcrop photographs of Upper Triassic sediments.
(a) Dark-grey siltstone in Rujigou area; (b, c) yellow sandstone in Shigouyi area; (d) grey sandstone in Baojishan area; (e) conglomerate in Kongtongshan area; (f) grey sandstone in Ankou area.

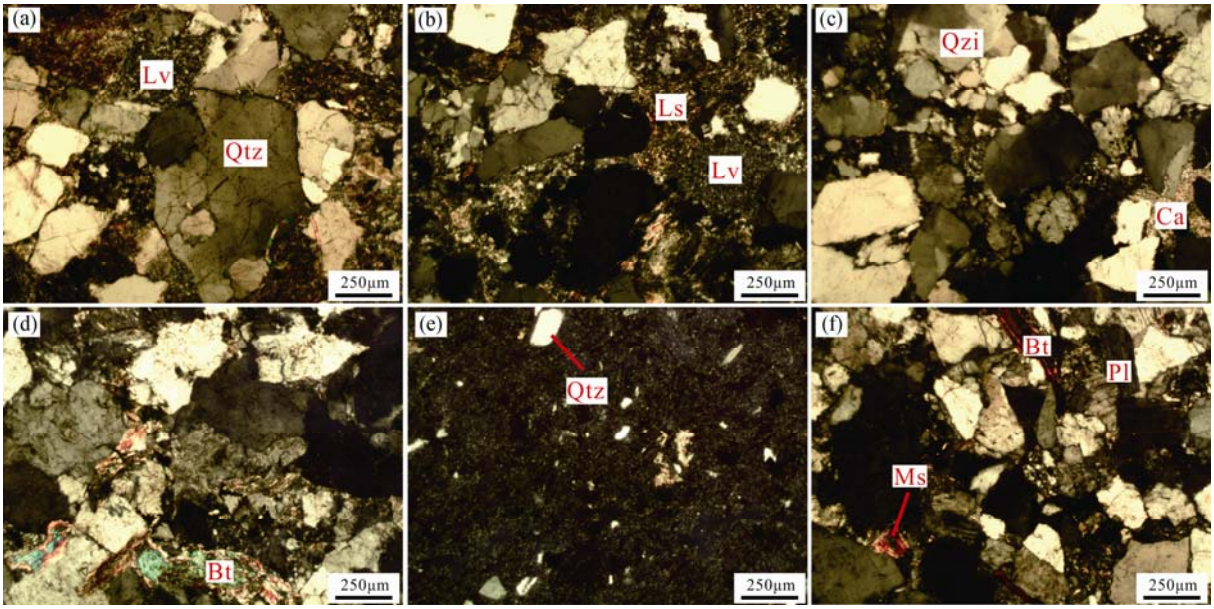

Fig. 3. Photomicrographs of the Upper Triassic sandstones from the western margin of Ordos Basin (crossed polars).
Quartz grain (Qtz); Volcanic lithic fragment (Lv); Sedimentary lithic fragment (Ls); Quartize fragment (Qzi); Calcite cement (Ca); Biotite mica grain (Bt); Plagioclase feldspar grain (Pl); Muscovite (Ms). (a) sample NW-1; (b) sample NW-3; (c) sample MW-1; (d) sample MW-10; (e) tuff in Baojishan area; (f) sample MW-7.

characterized by tuff layer (Fig. 3e), which could be comparable with that in Yanchang Formation of the Ordos Basin (Xin et al., 2013a). The whole set of greyish-green clastic rocks record an overall fluvial environment, occasionally coal streaks reveal a lacustrine setting.

Sandstone samples were sent to the Xi'an Institute of Geology and Mineral Resources for slices making, and thin sections were studied under a microscope by standard techniques to identify the minerals and for modal analyses at the Department of Geology, Northwest University, China. Based on the observation of thin sections, samples less affected by diagenesis would be selected for geochemical analysis. Major and trace elements of studied samples were analyzed at the State Key Laboratory of Continental Dynamics, Northwest University, China. Fresh chips of whole rock samples were powdered to 200 meshes using a tungsten carbide ball mill. Loss on ignition (LOI) was determined by heating samples to 950℃ for two hours. Major elements were analyzed using a Rikagu RIX 2100 X-ray Fluorescence Spectroscopy (XRF) and trace elements were analyzed by an Agilent 7500a inductively coupled plasma mass spectrometry (ICP-MS)

using United States Geological Survey (USGS) and international rock standards (BHVO-2, AGV-2, BCR-2 and GSP-1). For the trace element analysis, sample powders were digested using an $HF+HNO_3$ mixture in high-pressure Teflon bombs at 190°C for 48 hours. The analytical precision and accuracy for most of the major and trace elements are better than 5% and 10%, respectively (Liu et al., 2007). Results of the element analysis of the Upper Triassic sandstone samples from western Ordos Basin are displayed in Tables 1 and 2.

4 Results

4.1 Petrography of the sandstones

Petrographic identification was made on representative sandstone samples from the western Ordos Basin. Detrital grains include quartz, feldspars, rock fragments, micas, and heavy minerals (Figs. 3a–3f). Quartz is the predominant detrital grain and is of strained, unstrained and polycrystalline variety (Fig. 3). Most monocrystalline quartz grains are limpid with equant shapes and moderately undulose extinction. Feldspar crystals include plagioclase (Fig. 3f), orthoclase and microcline with plagioclase being the most common type of feldspar. Plagioclase feldspars exhibit polysynthetic twinning and minor sericitization occurring mainly on the surface. Potassium feldspars exhibit grid bicrystals and Carlsbad twin, which show hypidiomorphic granular texture. Mica including biotite and muscovite show strip shape or bending deformation (Fig. 3f), with the biotite being the dominant type. One tuff thin section from Baojishan area was also presented in Fig. 3e, which is matrix-supported and mainly composed of crystal, lithic and less altered vitric shards. The grain sizes for quartz, plagioclase, K-feldspar, biotite and muscovite range from 150 to 500 μm, from 150 to 400 μm, from 200 to 500 μm, from 200 to 500 μm, and from 80 to 250 μm, respectively, indicating fine-medium grained sandstones.

A large variety of igneous, sedimentary and metamorphic rock fragments are present in the Upper Triassic sandstones, of which the most common are described here. Among the igneous fragment, rhyolite and mafic volcanic fragments are common. Among the metamorphic rock fragments, quartzite is present (Fig. 3c). The sedimentary lithic fragments include sandstones, siltstones, mudstones and chert. Sandstone fragments are mostly quartzose. Chert fragments are also common and characterized by quartz granular aggregate.

The authigenic mineral of the sandstones, such as calcite, which forms interstitial cement was also showed in Fig. 3c. According to the observation on thin section, the sandstones are mainly clast-support type since the matrix concentration is relatively lower. Petrographic features show that the sandstones are characterized by low-medium compositional maturity and textural maturity.

4.2 Major elements

The major-element oxides in samples are SiO_2 (37.53 wt%–81.79 wt%) and Al_2O_3(6.24 wt%–17.3 wt%), and the TFe_2O_3, CaO, MgO, K_2O, and Na_2O are the second most abundant oxides, while all other oxides (TiO_2, P_2O_5 and MnO) are typically present at contents of<1 wt% (Table 1). The Al_2O_3/SiO_2 ratios range from 0.11 to 0.34 with four values greater than the Upper Continental Crust (UCC) average (0.23) (McLennan, 2001) (Table 1). This reflects the quartz enrichment and moderately mature nature of the sandstones (Kassi et al., 2015). The large variation in major element contents in samples from middle-western margin of Ordos Basin (MWM, including Shigouyi area and HCB) typifies weathered rocks. It is worth to note that the samples with lower SiO_2 and Al_2O_3 also contain higher CaO and LOI, indicating calcite being

Table 1 Concentrations of major-element oxides in sandstone samples from the western margin of Ordos Basin (wt%)

Sample no.	SiO_2	TiO_2	Al_2O_3	TFe_2O_3	CaO	Na_2O	K_2O	MgO	MnO	P_2O_5	LOI	Total	Al_2O_3/SiO_2	CIA	CIW	K_2O/Al_2O_3
NW-1	76.87	0.35	10.75	3.13	0.95	2.36	2.75	0.97	0.06	0.07	1.49	99.74	0.14	55.57	65.72	0.26
NW-2	75.79	0.42	10.67	3.31	1.00	2.51	2.50	1.29	0.03	0.08	2.16	99.74	0.14	55.20	64.22	0.23
NW-3	68.93	0.66	11.75	4.69	3.16	2.19	1.41	1.95	0.09	0.31	5.23	100.37	0.17	57.40	62.05	0.12
NW-4	70.75	0.32	11.68	3.36	3.07	2.92	1.20	1.32	0.05	0.15	4.73	99.55	0.17	51.70	54.87	0.10
NW-5	71.19	0.61	10.84	4.02	3.28	2.03	1.34	1.64	0.08	0.22	5.16	100.39	0.15	57.16	61.91	0.12
NW-6*	73.44	0.55	9.93	3.34	3.41	1.87	1.27	1.32	0.07	0.14	5.08	100.42	0.14	56.87	61.74	0.13
MW-1	66.22	0.50	12.37	5.76	3.64	1.13	2.59	1.37	0.27	0.14	5.63	99.61	0.19	65.53	76.97	0.21
MW-2	72.18	0.42	12.34	3.98	1.50	2.49	3.08	1.36	0.10	0.10	2.31	99.86	0.17	54.82	64.38	0.25
MW-3	70.19	0.45	12.35	4.57	2.21	2.04	2.92	1.36	0.16	0.11	3.42	99.78	0.18	55.61	64.84	0.24
MW-4	71.86	0.42	12.12	4.09	1.85	2.26	2.90	1.32	0.12	0.10	2.85	99.90	0.17	54.24	63.14	0.24
MW-5	69.55	0.46	11.92	4.80	2.91	1.57	2.56	1.29	0.20	0.12	4.50	99.85	0.17	60.00	69.76	0.21
MW-6*	64.23	0.53	12.38	6.35	4.35	0.67	2.42	1.37	0.33	0.15	6.74	99.52	0.19	71.93	84.88	0.20
MW-7	64.62	0.57	13.37	5.15	3.64	2.25	2.33	1.80	0.12	0.18	5.77	99.80	0.21	57.38	64.36	0.17
MW-8	43.73	0.6	14.87	5.69	1.13	1.03	1.97	1.59	0.03	0.69	28.92	100.25	0.34	71.63	79.85	0.13
MW-9	61.19	0.77	16.83	6.59	1.30	1.67	3.44	2.34	0.07	0.18	5.44	99.82	0.28	65.54	76.69	0.20
MW-10	81.79	0.16	9.22	1.17	0.25	2.04	3.14	0.42	0.03	0.03	1.29	99.54	0.11	56.09	70.75	0.34
MW-11	62.91	0.67	15.10	5.87	2.47	1.96	2.89	2.07	0.10	0.18	5.61	99.81	0.24	61.18	70.07	0.19
SW-1	76.90	0.33	8.92	3.03	2.24	0.65	2.60	1.23	0.05	0.08	3.56	99.59	0.12	64.27	80.66	0.29
SW-2	67.81	0.58	13.95	5.29	1.15	3.92	2.41	1.84	0.08	0.19	2.59	99.81	0.21	55.56	62.02	0.17
SW-3	61.11	0.75	17.30	5.96	1.20	2.38	3.24	2.74	0.08	0.13	4.34	99.23	0.28	64.27	73.93	0.19
SW-4	37.53	2.40	6.24	3.50	19.25	0.66	1.44	6.45	0.12	0.25	21.61	99.45	0.17	62.56	74.18	0.23
SW-5	57.72	1.20	11.24	6.40	4.64	1.52	1.82	6.33	0.06	0.16	8.41	99.50	0.19	61.70	69.21	0.16
SW-6	62.77	0.89	12.60	5.85	2.90	2.72	2.12	4.09	0.07	0.18	5.50	99.66	0.20	52.83	58.46	0.17
SW-7	61.45	0.37	7.29	2.85	10.70	0.35	2.33	2.68	0.06	0.13	11.80	99.97	0.12	66.59	86.53	0.32
SW-8	59.06	0.49	7.23	1.48	14.46	0.14	2.70	0.64	0.03	0.19	13.17	99.57	0.12	68.17	94.21	0.37
SW-9	55.98	0.84	9.25	4.07	10.77	0.88	2.28	3.53	0.05	0.17	11.77	99.55	0.17	63.35	76.25	0.25

LOI - loss on ignition; CIA - chemical index of alteration; CIW - chemical index of weathering; *data is from Yang et al. (2011).

Table 2Concentrations of trace elements and REEs in sandstone samples from the western margin of Ordos Basin (ppm)

Sample	Sc	V	Cr	Co	Ni	Cu	Zn	Rb	Sr	Y	Zr	Nb	Cs	Ba	Hf	Ta	Th	U	V/Cr	Ni/Co	Th/Sc	C-value
NW-1	6.66	44.95	36.30	116.75	13.50	5.94	33.70	77.68	210.75	15.93	152.50	7.83	1.32	729.25	3.99	0.72	10.43	1.25	1.24	0.12	1.56	0.42
NW-2	6.70	47.15	47.05	116.00	14.40	4.63	33.10	73.10	209.50	16.05	205.00	9.29	1.33	737.50	5.26	0.87	10.85	1.46	1.00	0.12	1.62	0.43
NW-3	8.67	55.03	51.38	89.83	18.55	9.70	48.03	55.05	179.75	27.08	396.25	12.45	1.84	349.50	10.01	1.02	13.88	2.71	1.07	0.21	1.60	0.54
NW-4	4.11	31.20	28.15	136.45	20.24	5.56	35.95	54.60	147.55	12.45	151.00	5.04	1.30	305.00	3.94	0.39	6.90	1.61	1.11	0.15	1.68	0.39
NW-5	7.02	47.11	45.64	114.91	15.18	7.31	41.01	53.03	198.88	22.39	425.13	11.63	1.51	315.75	10.60	1.02	15.79	1.98	1.03	0.13	2.25	0.48
NW-6*	5.37	39.20	39.90	140.00	11.80	4.91	34.00	51.00	218.00	17.70	454.00	10.80	1.18	282.00	11.20	1.02	17.70	2.72	0.98	0.08	3.30	0.42
Av	6.42	44.11	41.40	118.99	15.61	6.34	37.63	60.74	194.07	18.60	297.31	9.50	1.41	453.17	7.50	0.84	12.59	1.96	1.07	0.13	2.0	0.45
EF	0.47	0.41	0.50	7.00	0.35	0.25	0.53	0.54	0.55	0.85	1.56	0.79	0.31	0.82	1.29	0.84	1.18	0.70	—	—	—	—
MW-1	8.11	58.38	51.35	48.88	23.63	9.80	51.03	79.50	169.00	18.25	191.50	8.29	2.39	601.75	5.00	0.65	8.81	1.88	1.14	0.48	1.09	0.66
MW-2	6.9	49	38	9.2	15.3	6.8	43	87.9	247	12.4	148	6.5	2.30	730	3.9	0.50	7.68	1.3	1.29	1.66	1.11	0.45
MW-3	7.30	52.13	42.45	22.43	18.08	7.80	45.68	85.10	221.00	14.35	162.50	7.10	2.33	687.25	4.27	0.55	8.06	1.49	1.23	0.81	1.10	0.52
MW-4	7.35	50.39	40.53	41.51	16.51	7.10	42.19	82.83	221.25	14.33	148.75	7.08	2.15	713.13	3.94	0.58	8.36	1.37	1.24	0.40	1.14	0.47
MW-5	8.21	54.90	47.50	87.05	20.50	8.41	44.05	74.95	169.50	18.20	164.00	8.25	2.02	653.50	4.34	0.70	9.42	1.64	1.16	0.24	1.15	0.57
MW-6*	8.51	61.50	55.80	62.10	26.40	10.80	53.70	76.70	143.00	20.20	206.00	8.88	2.42	559.00	5.37	0.70	9.18	2.07	1.10	0.43	1.08	0.73
MW-7	11.2	75.9	72.9	26.0	34.7	19.3	70.5	82.5	201	23.7	170	9.58	3.03	613	4.34	0.67	7.93	2.13	1.04	1.33	0.71	0.50
MW-8	14.5	144	72.7	37.1	44.7	82.8	97.0	106	135	33.8	116	9.20	6.89	339	3.05	0.63	11.7	9.22	1.97	1.20	0.81	0.96
MW-9	16.6	112	94.8	21.7	46.6	41.4	98.9	140	155	30.9	188	12.9	6.49	623	4.57	0.87	12.1	3.54	1.18	2.15	0.73	0.72
MW-10	2.61	19.3	12.3	50.0	6.75	2.02	16.1	81.8	112	6.26	80.6	4.23	1.04	788	1.99	0.56	6.23	1.09	1.57	0.14	2.38	0.18
MW-11	13.86	93.86	83.85	23.83	40.66	30.34	84.73	111.21	178.37	27.31	179.23	11.25	4.76	618.09	4.45	0.77	10.01	2.83	1.12	1.71	0.72	0.61
Av	9.56	70.07	55.66	39.07	26.71	20.59	58.82	91.65	177.52	19.97	159.55	8.48	3.26	629.66	4.11	0.65	9.04	2.60	1.26	0.68	1.09	0.58
EF	0.70	0.65	0.67	2.30	0.61	0.82	0.83	0.82	0.51	0.91	0.84	0.71	0.71	1.14	0.71	0.65	0.85	0.93	—	—	—	—
SW-1	4.9	38	29	5.1	10.8	9.9	43	80.4	83.6	10.2	116	6.7	2.18	560	3.3	0.64	7.77	1.5	1.31	2.12	1.59	0.43
SW-2	9.8	70	60	14.8	26.7	16.5	79	79.4	180.0	18.2	155	9.5	2.89	660	4.4	0.71	8.26	1.8	1.17	1.80	0.84	0.55
SW-3	15.4	100	79	15.1	36.9	38.1	94	141.5	212	23.7	192	12.5	7.36	570	5.5	0.92	14.00	3.5	1.27	2.44	0.91	0.61
SW-4	11.4	111	62	9.9	14.2	18.2	50	44.4	171.0	40.1	1430	25.7	1.06	390	14.7	1.54	21.1	3.8	1.79	1.43	1.85	0.13
SW-5	15.6	133	69	18.6	33.0	49.9	62	55.5	116.5	21.5	238	12.5	1.51	440	6.5	0.80	8.09	2.1	1.93	1.77	0.52	0.46
SW-6	12.70	101.50	64.50	16.70	29.85	33.20	70.50	67.45	148.25	19.85	196.50	11.00	2.20	550.00	5.45	0.76	8.18	1.95	1.57	1.79	0.64	0.50
SW-7	5.80	45.10	34.80	6.02	12.45	11.79	51.43	95.76	98.36	12.09	136.98	7.68	2.68	657.90	3.90	0.78	9.08	1.80	1.30	2.07	1.57	0.18
SW-8	8.40	65.20	51.20	9.87	18.67	17.23	76.31	127.78	135.91	18.23	189.67	10.65	4.01	789.54	5.02	1.06	13.75	2.10	1.27	1.89	1.64	0.08
SW-9	17.10	146.10	76.10	19.50	36.20	54.90	68.20	60.10	127.90	23.60	261.00	13.80	1.60	485.00	7.10	0.84	8.90	2.40	1.92	1.86	0.52	0.23
Av	11.23	89.99	58.40	12.84	24.31	27.75	66.05	83.59	141.50	20.83	323.91	12.23	2.83	566.94	6.21	0.89	11.01	2.33	1.54	1.89	1.12	0.35
EF	0.83	0.84	0.70	0.76	0.55	1.11	0.93	0.75	0.40	0.95	1.70	1.02	0.62	1.03	1.47	0.89	1.03	0.83	—	—	—	—
UCC	14	107	83	17	44	25	71	112	350	22	190	12	4.6	550	5.8	1	10.7	2.8	1.29	2.59	0.76	—

REEs

Sample	La	Ce	Pr	Nd	Sm	Eu	Gd	Tb	Dy	Ho	Er	Tm	Yb	Lu	LREE	HREE	L/HREE	∑REE	δEu	δCe	$(La/Sm)_N$	$(Gd/Yb)_N$	$(La/Yb)_N$
NW-1	34.80	66.60	7.34	25.88	4.47	1.12	4.07	0.55	2.93	0.58	1.55	0.22	1.56	0.23	140.20	11.69	12.00	151.89	0.80	1.00	4.90	2.10	15.04
NW-2	38.00	71.80	7.93	27.60	4.78	1.06	4.29	0.58	3.09	0.60	1.64	0.23	1.63	0.24	151.17	12.29	12.30	163.46	0.71	1.00	5.00	2.12	15.72
NW-3	42.83	83.15	9.60	34.50	6.17	1.32	5.77	0.80	4.48	0.92	2.57	0.36	2.50	0.37	177.56	17.76	10.00	195.32	0.68	0.99	4.37	1.86	11.55
NW-4	23.30	45.40	5.18	18.30	3.32	0.76	3.02	0.42	2.29	0.46	1.24	0.18	1.25	0.19	96.26	9.04	10.65	105.30	0.73	0.99	4.41	1.95	12.57
NW-5	45.71	87.58	10.00	35.40	6.19	1.18	5.51	0.73	3.92	0.78	2.15	0.30	2.11	0.32	186.06	15.82	11.76	201.88	0.62	0.99	4.64	2.11	14.61
NW-6*	48.60	92.00	10.40	36.30	6.22	1.04	5.25	0.67	3.36	0.64	1.73	0.24	1.72	0.26	194.56	13.87	14.03	208.43	0.56	0.98	4.91	2.46	19.05
Av	38.87	74.42	8.41	29.66	5.19	1.08	4.65	0.63	3.34	0.66	1.81	0.26	1.80	0.27	157.63	13.41	11.79	171.04	0.68	0.99	4.71	2.10	14.75
EF	1.30	1.16	1.18	1.14	1.15	1.22	1.22	0.98	0.96	0.83	0.79	0.77	0.82	0.83	—	—	—	—	—	—	—	—	—
MW-1	28.38	55.83	6.20	22.00	4.00	0.91	3.64	0.53	3.08	0.65	1.81	0.27	1.86	0.28	117.31	12.12	9.68	129.43	0.73	1.01	4.46	1.58	10.27
MW-2	29.50	59.80	6.05	21.70	3.69	0.85	2.91	0.42	2.43	0.48	1.31	0.19	1.27	0.20	121.59	9.21	13.20	130.80	0.79	1.08	5.03	1.85	15.66
MW-3	29.13	58.48	6.10	21.80	3.79	0.87	3.15	0.46	2.65	0.54	1.48	0.22	1.47	0.23	120.16	10.18	11.80	130.34	0.77	1.06	4.83	1.73	13.38
MW-4	31.64	62.44	6.59	23.33	4.00	0.91	3.36	0.48	2.71	0.54	1.49	0.22	1.48	0.23	128.90	10.51	12.26	139.41	0.76	1.04	4.98	1.83	14.38
MW-5	33.40	63.75	7.18	25.05	4.41	0.99	4.05	0.57	3.22	0.66	1.85	0.27	1.90	0.28	134.78	12.78	10.55	147.56	0.72	0.99	4.76	1.72	11.88
MW-6*	28.00	54.50	6.25	22.10	4.10	0.93	3.88	0.57	3.30	0.70	1.98	0.29	2.06	0.31	115.88	13.09	8.85	128.97	0.71	0.99	4.30	1.52	9.16
MW-7	30.44	61.71	7.09	27.36	5.34	1.23	4.94	0.71	4.13	0.79	2.29	0.33	2.15	0.32	133.17	15.66	8.51	148.82	0.73	1.01	3.59	1.85	9.54
MW-8	43.86	76.76	8.40	31.93	6.00	1.35	5.86	0.82	4.77	0.93	2.72	0.37	2.45	0.36	168.31	18.27	9.21	186.58	0.69	0.96	4.60	1.93	12.09
MW-9	37.50	72.90	8.63	32.77	6.29	1.38	5.70	0.83	5.01	0.99	2.90	0.41	2.75	0.40	159.46	19.00	8.39	178.46	0.71	0.98	3.75	1.67	9.18
MW-10	12.33	23.72	2.67	9.50	1.65	0.47	1.35	0.19	1.08	0.22	0.67	0.10	0.72	0.11	50.34	4.43	11.35	54.78	0.96	0.99	4.70	1.52	11.58
MW-11	33.97	67.30	7.86	30.06	5.81	1.31	5.32	0.77	4.57	0.89	2.59	0.37	2.45	0.36	146.31	17.33	8.44	163.64	0.72	0.99	3.68	1.75	9.34
Av	30.74	59.74	6.64	24.33	4.46	1.02	4.01	0.58	3.36	0.67	1.92	0.28	1.87	0.28	126.93	12.96	10.20	139.89	0.75	1.01	4.42	1.72	11.50
EF	1.02	0.93	0.93	0.94	0.99	1.16	1.06	0.90	0.96	0.84	0.83	0.84	0.85	0.87	—	—	—	—	—	—	—	—	—
SW-1	22.70	44.30	4.50	16.50	2.99	0.66	2.38	0.35	2.11	0.43	1.17	0.17	1.15	0.17	91.65	7.93	11.56	99.58	0.76	1.05	4.78	1.67	13.31
SW-2	28.70	60.20	6.44	24.40	4.65	1.03	4.16	0.59	3.46	0.69	1.87	0.27	1.72	0.27	125.42	13.03	9.63	138.45	0.72	1.07	3.88	1.95	11.25
SW-3	49.00	95.90	9.64	35.00	6.32	1.23	5.26	0.77	4.71	1.03	2.86	0.41	2.68	0.41	197.09	18.13	10.87	215.22	0.65	1.06	4.88	1.58	12.33
SW-4	61.60	127.00	13.65	50.50	9.29	1.79	8.58	1.31	8.50	1.79	5.39	0.77	5.22	0.80	263.83	32.36	8.15	296.19	0.61	1.05	4.17	1.33	7.96
SW-5	31.50	65.20	7.11	26.80	4.94	1.14	4.54	0.71	4.38	0.91	2.57	0.36	2.34	0.36	136.69	16.17	8.45	152.86	0.74	1.05	4.01	1.57	9.08
SW-6	30.10	62.70	6.78	25.60	4.80	1.09	4.35	0.65	3.92	0.80	2.22	0.32	2.03	0.32	131.06	14.60	8.98	145.66	0.73	1.06	3.95	1.73	10.00
SW-7	22.92	44.32	4.96	18.69	3.49	0.74	3.04	0.44	2.76	0.59	1.63	0.24	1.52	0.24	95.10	10.43	9.12	105.53	0.69	1.00	4.14	1.62	10.20
SW-8	33.54	63.70	7.39	27.44	5.17	1.04	4.74	0.64	4.22	0.92	2.64	0.39	2.50	0.40	138.27	16.44	8.41	154.70	0.64	0.97	4.08	1.53	9.06
SW-9	31.74	63.13	7.16	26.78	4.95	1.09	4.58	0.67	4.29	0.90	2.56	0.37	2.35	0.37	134.84	16.06	8.40	150.90	0.70	1.01	4.03	1.58	9.12
Av	34.64	69.60	7.51	27.97	5.18	1.09	4.62	0.68	4.26	0.90	2.54	0.37	2.39	0.37	145.99	16.13	9.05	162.12	0.69	1.04	4.21	1.62	10.26
EF	1.15	1.09	1.06	1.08	1.15	1.24	1.22	1.06	1.22	1.12	1.11	1.11	1.09	1.15	—	—	—	—	—	—	—	—	—
UCC	30	64	7.1	26	4.5	0.88	3.8	0.64	3.5	0.8	2.3	0.33	2.2	0.32	132.48	13.89	9.54	146.37	0.65	1.08	4.3	1.43	9.78

Note: $\delta Eu=Eu_N/(Sm_N\times Gd_N)^{1/2}$;$\delta Ce = Ce_N/(La_N\times Pr_N)^{1/2}$, N stands for chondrite normalized values, the chondrite data are from Sun and McDonough, 1989;*data is from Yang et al. (2011).

the most likely reason for the elemental correlation.

In the northwestern margin of Ordos Basin (NWM), most of the major element contents present a positive co-variation with the Al_2O_3 abundances with the exception of SiO_2 and K_2O (Fig. 4). While in the MWM, the Al_2O_3 abundances only display a positive co-variation with the contents of TiO_2, TFe_2O_3, MgO and P_2O_5 (Fig. 4), these correlations indicate that the influence of clay minerals (because the Al_2O_3 contents are related to the clay minerals), and other elements are related to redox conditions or involve other origins such as volcanic ashes or hydrothermal fluids. Similarly, in the southwestern margin of Ordos Basin (SWM), the Al_2O_3 abundances only display a positive co-variation with the contents of SiO_2, TFe_2O_3, Na_2O and K_2O (Fig. 4).

4.3 Trace elements

The trace element contents of sandstone samples are presented in Table 2. Table 2 also contains the concentrations of trace elements in UCC (McLennan, 2001) and average enrichment factor (EF). On average, the most abundant trace elements in the Upper Triassic sandstones are Ba (567.22 ppm), Zr (248.23 ppm), and Sr (168.87 ppm), whereas all the other elements occur in amounts smaller than 100 ppm.

In order to quantitatively evaluate the degree of element enrichment compared to the average of UCC, Patterson et al. (1986) used EF, which was defined as the ratio of the element concentration in samples to the corresponding concentration in the UCC. As shown in Table 2, Co is mostly enriched in NWM, with EF ranging from 5.28 to 8.03 (av. 7.0). Zr is enriched in NWM and SWM, with EF averages of 1.56 and 1.7, respectively. Hf also shows enrichment in NWM and SWM, with EF averages of 1.29 and 1.47, respectively. Different from the elements above, Ba is enriched in MWM, with EF average of 1.14. The remaining trace elements show more or less the same content as their UCC values with the EF between 0.25 and 1.18.

4.4 Rare earth elements

The average REE contents of sandstones from NWM, MWM, and SWM are 171.04 ppm, 139.89 ppm and 162.12 ppm, respectively, which are comparable to that of the UCC (McLennan, 2001). The light rare earth elements (LREEs) are enriched, while the EF values of heavy rare earth elements (HREEs) are less than 1.0 and are relatively lower in NWM and MWM than those in SWM. In addition, the LREEs abundances are higher than HREEs, with the L/HREE and $(La/Yb)_N$ ratios decreasing from north to south. These indicators reflect the stronger fractionation of LREEs and HREEs in NWM. The $(La/Sm)_N$ ranges from 3.59 to 5.03, with an average of 4.42, and the $(Gd/Yb)_N$ varies between 1.33 and 2.46, with an average of 1.77, suggesting the LREEs are more fractionated than the HREEs. As shown in the chondrite-normalized REE distribution patterns (Figs. 5a–5c), all of the samples show LREE enrichment and right-oblique curves. The LREE segments show a more obvious right obliquity, while the HREE segments are relatively smooth. The value of δEu ranges from 0.56 to 0.96, with an average of 0.72. And the value of δCe ranges from 0.96 to 1.08, with an average of 1.01. These features indicate an overall moderate negative Eu anomaly and a slightly positive Ce anomaly, respectively. In general, granite is characterized by negative Eu anomaly (Zhang and Zhang,

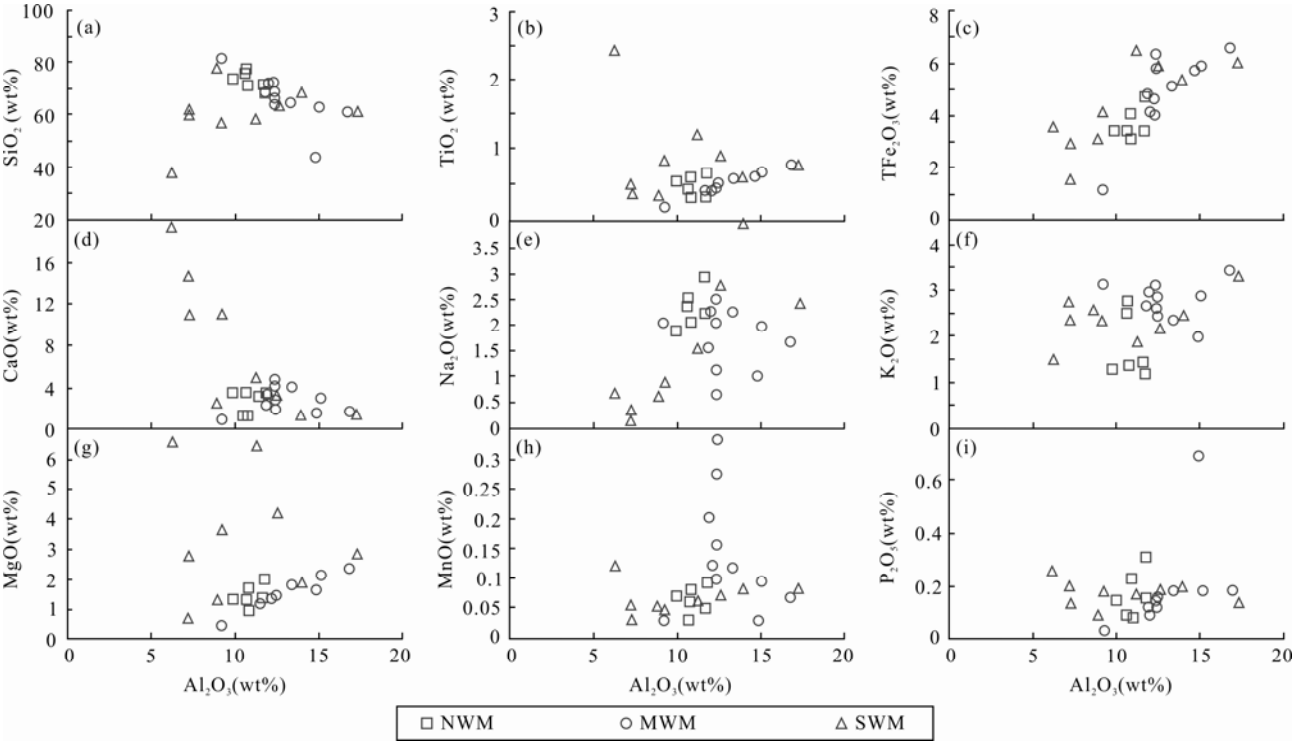

Fig. 4. Correlation diagram of Al_2O_3 with other major element oxides.

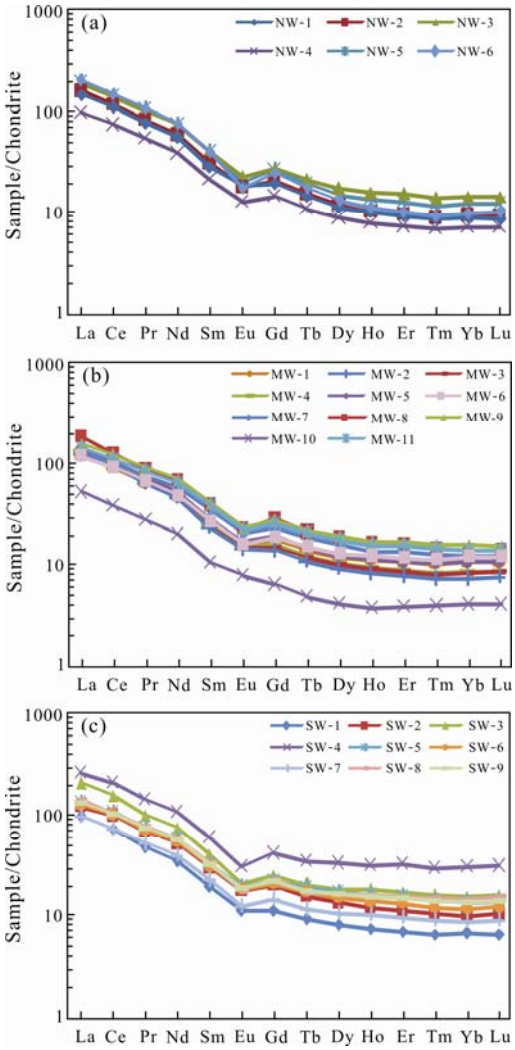

Fig. 5. Chondrite-normalized REE diagram for the Upper Triassic sandstones in NWM (a), MWM (b), and SWM (c). Chondrite data from Sun and McDonough, 1989.

2007), which implies that the source rock might be derived from acid igneous rocks. Aubert et al. (2001) have determined that weathering of granitic rocks does not appear to result in any Ce anomalies in the weathering products. A larger range in Ce anomalies in MWM and SWM relative to NWM may be attributed to the contribution of weathered material derived from a mixed source.

5 Discussions

5.1 Weathering in the source areas

The Chemical Index of Alteration (CIA) and the Chemical Index of Weathering (CIW) are useful measures of degree to constrain chemical weathering history from the source area (Nesbitt and Young, 1982; McLennan et al., 1993; Shi et al., 2016; Lewin et al., 2018). High CIA and CIW values often indicate strong weathering characteristics. In general, intensive chemical weathering results in residual clays such as kaolinite and gibbsite, with CIA values of 76–100. CIA values in shales range between ~65 and ~75, reflecting muscovite, illite and smectite compositions and indicating a moderately weathered source, while those between ~50 and ~65 indicate weak weathering history. Fresh igneous rocks and feldspar have average CIA values of ~50 or≤50 indicating unweathered source areas (Nesbitt and Young, 1982).

Using molecular proportions: $CIA=Al_2O_3/(Al_2O_3+K_2O+Na_2O+CaO^*)\times 100$, which was defined by Nesbitt and Young (1982). The $CIW=Al_2O_3/(Al_2O_3+Na_2O+CaO^*)\times 100$, which was defined by Harnois (1988). CaO* is the amount of CaO incorporated into the silicate fraction of rocks (Nesbitt and Young, 1982). In this study, the CaO was initially corrected for phosphate using available P_2O_5 data ($CaO^*=CaO-P_2O_5\times 10/3$). If the remaining number of moles is less than that of Na_2O, the CaO value was adopted as the CaO*. Otherwise, the CaO* was assumed to be equivalent to Na_2O (McLennan et al. 1993). The CIA values of the analytical samples range from 51.7 to 71.93, with an average of 60.28, and the CIW values vary between 54.87 and 94.21, with a mean of 70.45 (Table 1), both of the two indices are comparable with that of the UCC (60.11 and 70.89, respectively, McLennan, 2001). In Fig. 6, most samples fall in the weak weathering area, which probably reflects the presence of immature sands containing relatively fresh detrital feldspars and point to a relatively unweathered source. Only four samples from MWM and two samples from SWM fall in the intermediate weathering area (CIA value higher than 65, Fig. 6), reflecting the presence of mature sands containing relatively unfresh detrital feldspars from a relatively weathered or a tectonically inactive source (Saminpanya et al., 2014). The data spread suggests the sediments could come from different chemical weathering sources.

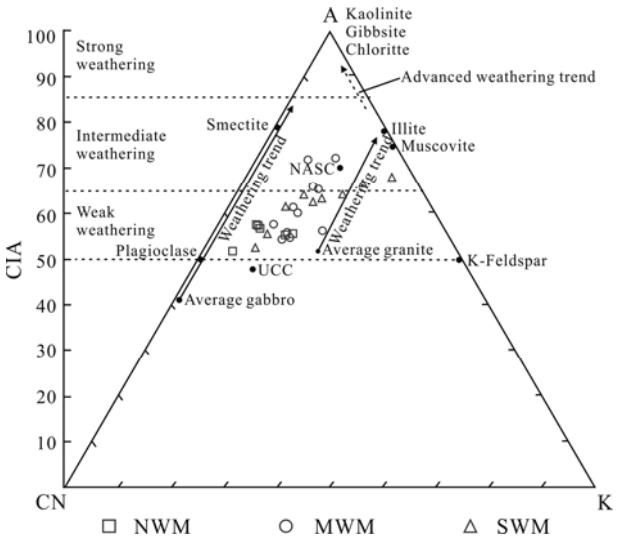

Fig. 6. Chemical Index of Alteration (CIA) with ternary diagram, A–CN–K (Al_2O_3 – CaO* + Na_2O – K_2O) (after Nesbitt and Young, 1982, 1984, 1989) of the Upper Triassic sandstones in western margin of Ordos Basin. The CIA values estimate the degree of chemical weathering of the clastic fractions. Arrows indicate the general trends of weathering.

5.2 Provenance

The geochemical components of detrital rocks are controlled by their provenance and thus can directly reflect the composition of the parent rocks (Cullers, 1994; Whitmore et al. 2004). To infer provenance, discriminant function scores of the samples (F1 and F2) for major elements were plotted within the fields proposed by Roser and Korsch (1988) (Fig. 7). The samples from NWM mainly lie in the field of quartzose sedimentary provenance (Fig. 7), this field represents recycled-mature polycyclic quartzose detritus and the recycled sources represent quartzose sediments of mature continental provenance. The samples from MWM lie mainly in the field of felsic igneous provenance (Fig. 7), while the samples from SWM lie mainly in the field of quartzose sedimentary provenance (Fig. 7), except for two samples falling in felsic igneous provenance. Fig. 7 indicates that the samples from NWM and SWM were reworked or recycled from older sediments (Diskin et al., 2011). The recycled nature of those sediments is also reflected in the higher Zr and Hf contents.

High field strength elements (HFSE), e.g., Zr, Nb, Y, Th, and Sc are well suited for provenance determinations because of their relatively low mobility during sedimentary processes (weathering, transport, diagenesis) and metamorphism, and their low residence time in sea water/water columns (Holland, 1978). They are transported quantitatively into clastic sedimentary rocks during weathering and transportation and provide a signature of the parent material (McLennan et al., 1983; Cullers, 1994, 2000; Cox et al., 1995; Cullers and Podkovyrov, 2000, 2002). In general, Th abundance is higher in felsic than in mafic igneous source rocks and in their weathered products, whereas Sc and Cr are more concentrated in mafic than in felsic igneous rocks and in their weathered products (Taylor and McLennan, 1985; Wronkiewicz and Condie, 1987). The relative enrichments of incompatible elements, e.g., Th over Sc in the sediments, indicate relatively felsic average provenance compositions. Similarly, the geochemical differences between elements such as Th and La (indicative of a felsic source) and Sc and Cr (indicative of a mafic source) have also been exploited to distinguish between felsic and mafic provenance (e.g., Wronkiewicz and Condie, 1990).

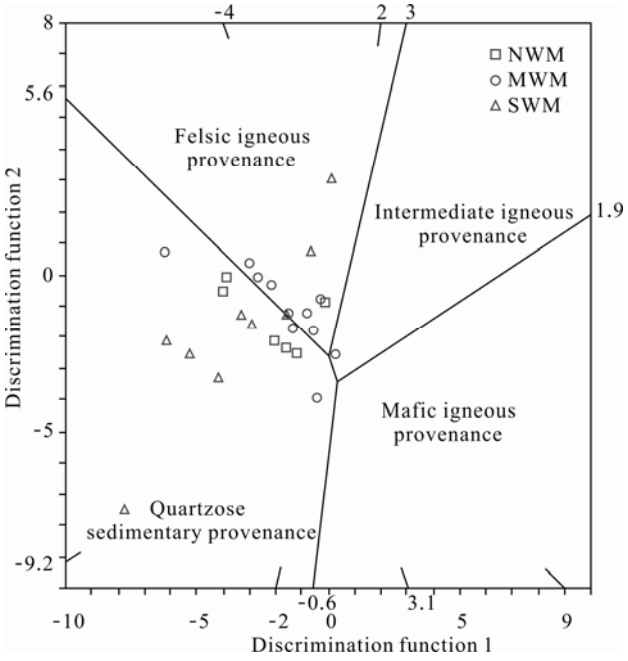

Fig. 7. Plot of discrimination functions 1 (=–1.773TiO_2+0.607Al_2O_3+0.76Fe_2O_3(toc)–1.5MgO+0.616CaO+0.509Na_2O–1.224K_2O–9.09) vs. 2 (=0.445TiO_2+0.07Al_2O_3–0.25Fe_2O_3(toc) –1.142MgO+0.438CaO+1.475Na_2O+1.426K_2O–6.861), after Roser and Korsch, 1988.

In this study, the Th/Sc ratios range from 0.52 to 3.3, the average values of samples in NWM, MWM, and SWM are 2.00, 1.09, and 1.12, respectively, which are similar to UCC value (Table 2), suggesting contribution from a felsic source. The Th vs. Sc plot (Fig. 8a) shows that most sediment data scatter above the Th/Sc=1 line, indicating a more felsic component (Nyakairu and Koeberl, 2001). The minor data group plots in the area between Th/Sc=0.6 and 1, and two samples from SWM have Th/Sc<0.6. This indicates that the sediments did not reflect a uniform provenance but a mixed source. Some sediment data plot close to the value of UCC, this result is consistent with low level of weathering condition (Fig. 6). Moreover, the studied sediments show non-uniform K/Rb ratios (Fig. 8b, after Shaw, 1968), in that, most samples lie close to a typical differentiated magmatic suite or main trend with a ratio of 230. Certain samples have lower K/Rb values. This feature emphasizes the chemically coherent nature of the sediments and derivation mainly from acidic to intermediate rocks.

Th/Sc-Zr/Sc diagram is a useful index of zircon enrichment (McLennan et al. 1993). Zircons accumulate during sedimentation while less resistant phases are preferentially destroyed. The Zr/Sc ratio is a useful tracer for zircon or heavy mineral concentration (Taylor and McLennan, 1985). In first-cycle sediments, Th/Sc ratios show an overall positive correlation with Zr/Sc, depending on the nature of the source rock. In contrast, Zr/Sc ratios in mature or recycled sediments display considerable variation with little change in the accompanying Th/Sc ratio (McLennan et al. 1993), indicating zircon addition due to sediment recycling (Fig. 9a). Some lower values in the diagram show the simple correlation ratios and agree well with the compositional variation trend. This indicates lessened effect of sedimentary process, with the higher values from enrichments of zircon (high Zr/Sc ratio) resulting from sedimentary sorting and recycling. This pattern is attributed to compositional variations. The Zr/Sc ratios of samples from NWM are obviously higher than others, suggesting a higher concentration of zircon (and significant sediments recycling) in the former, the recycled nature of sediments in NWM is also suggested by Fig. 7. Other trace element characteristics of sedimentary rocks also place some constraints on the nature of the source. Floyd and Leveridge (1987) used a La/Th vs. Hf plot to discriminate between different source compositions. In Figure 9b, most data of the sandstones fall in the felsic source field with a few data fall in mixed felsic/basic source, while a few samples in Rujigou are supposed to be derived from increasing old sediment component. The Hf

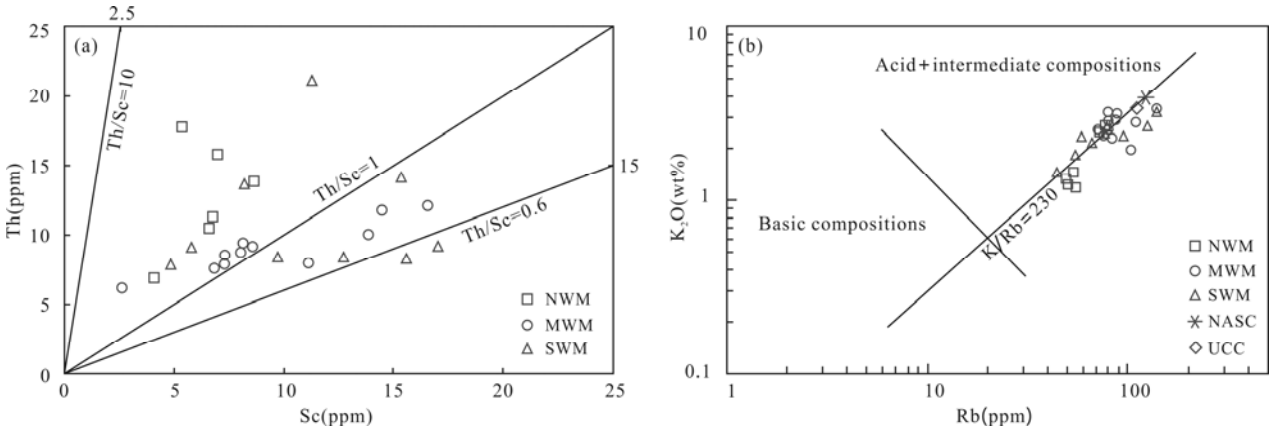

Fig. 8. (a) Th vs. Sc for rock samples. Th/Sc=1 ratio represents the average Upper Continental Crust (UCC) (data from Taylor and McLennan, 1985). (b) Distribution of K and Rb in the samples relative to a K/Rb ratio of 203 (=main trend of Shaw, 1968).

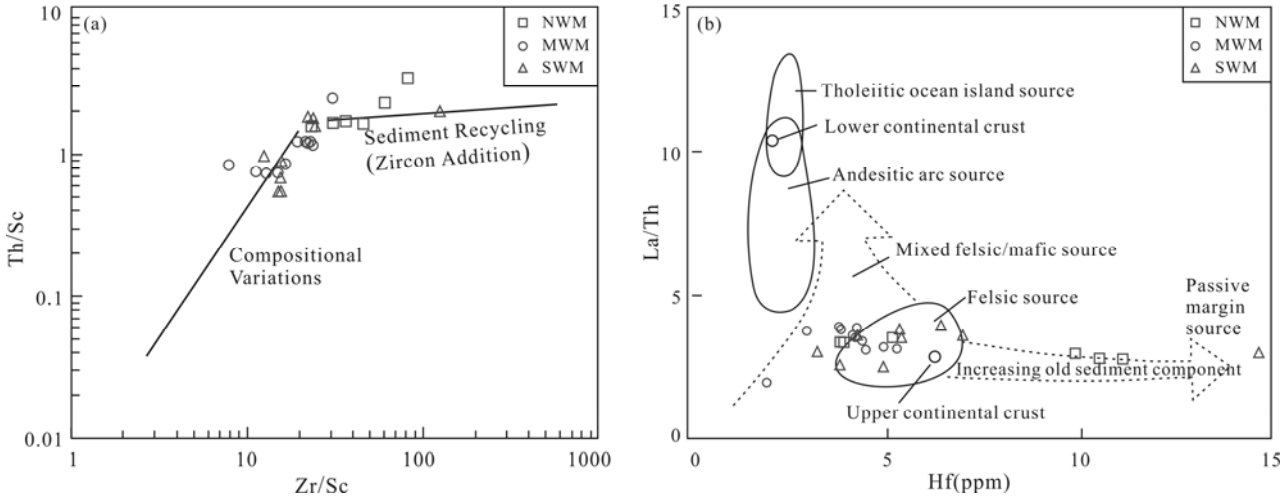

Fig. 9. (a) Plot of Th/Sc vs. Zr/Sc for the samples (after McLennan et al., 1993). The line in the lower part shows the compositional variation trend which indicates a reduced effect of sedimentary process. The arrowed line indicates the sediment recycling (zircon addition) or high Zr/Sc ratio resulting from sedimentary sorting and recycling. (b) Source rock discrimination diagrams for sandstones on plot of La/Th vs. Hf (after Floyd and Leveridge, 1987).

contents of most samples in MWM are obviously lower than that of the other sandstones, which indicates the sediment recycling in MWM is less significant than other sandstones.

To better constrain the source, we measured the palaeocurrent data mainly by well-exposed cross-bedding and gravel fabric in the outcrop. Paleocurrent measurements were carried out following the method proposed by DeCelles et al. (1983). All measurements have been corrected for declination. These new data, together with previous published data (e.g., Li, 2006; Liu, 2009), were used to indicate the directions of paleocurrent. Results showed that to the northwest, flow directions are southeastward and southwestward; to the west, flow directions point to southeast and east in Shigouyi area and to southeast and northeast in HCB, while to the southwest, the flow directions are northeastward and eastward, indicating three primary flow directions (Fig. 1b). On the basis of palaeocurrent analysis, the REE data from surrounding possible source areas are presented for comparison. REE distribution patterns are usually considered as an important tracer for source rocks, because the REE concentrations are relatively immobile during the weathering and diagenetic processes (McLennan et al., 1993). The distribution pattern of the Upper Triassic sediments in NWM is similar to the magmatic rocks in Alxa Block, while that of the sediments from MWM and SWM are similar to the granite and metaclastics in Qinling-Qilian Belt. In addition, the gravel compositions of the conglomerate in Cedipo section (SWM) are characterized by meta-basic volcanic rocks, siliceous and granites with a few carbonate rocks, which is similar with the Longshan, Liziyuan and Huluhe group strata in the Qinling-Qilian Orogenic Belt.

Based on petrology, geochemistry and palaeocurrent evidence, we conclude that the provenance of NWM was mainly from the Alxa Block with a typical recycling nature, while the provenance of MWM and SWM were mainly from the Qinling-Qilian Orogenic Belt. Comparing samples from NWM, MWM, and SWM areas with various

lithologies from ancient land surrounding the western basin, this study shows sandstones in different areas could match well with different lithologies from ancient land surrounding the western basin, reflecting the differences in source rocks and tectonic features.

5.3 Tectonic implications

5.3.1 Tectonic setting of the provenance

Several classifications attempt to discriminate various origins and tectonic settings (Bhatia, 1983; Bhatia and Crook, 1986). Bhatia (1983) proposed discrimination diagrams using major element data to infer the tectonic setting of parent rocks. Within their study, they used TiO_2 vs. Fe_2O_3+MgO and Al_2O_3/SiO_2 vs. Fe_2O_3+MgO to define fields representing oceanic island arc (OIA), continental island arc (CIA), active continental margin (ACM) and passive margin (PM) tectonic settings. In this study, Figs. 10a and b represent distribution of the data from the Upper Triassic sandstones of the study area. Most of the studied samples fall in/near the general area of CIA and ACM, leaving a few points outside these fields. Trace elements, such as La, Th, Sc and Zr, are also useful fingerprints for chemical discrimination of tectonic setting (Bhatia and Crook, 1986). On the La-Th-Sc plot (Fig. 10c), all samples from Rujigou area (NWM) plot in the ACM and PM fields, most of the samples from MWM and SWM fall in the CIA field, with two samples outside these fields, falling in the transition area between the CIA and ACM/PM fields. Furthermore, in the Th-Sc-Zr/10 plot (Fig. 10d), the sandstones from Rujigou fall in the CIA and PM fields, while the samples from MWM and SWM mainly fall in the CIA field. Viewed in combination, these discrimination diagrams suggest that the parent rocks of the MWM and SWM sandstones were mainly derived from CIA, while the different distribution of the NWM samples in different discrimination diagrams reflects a complex nature.

During the Triassic, the subduction and final closure of

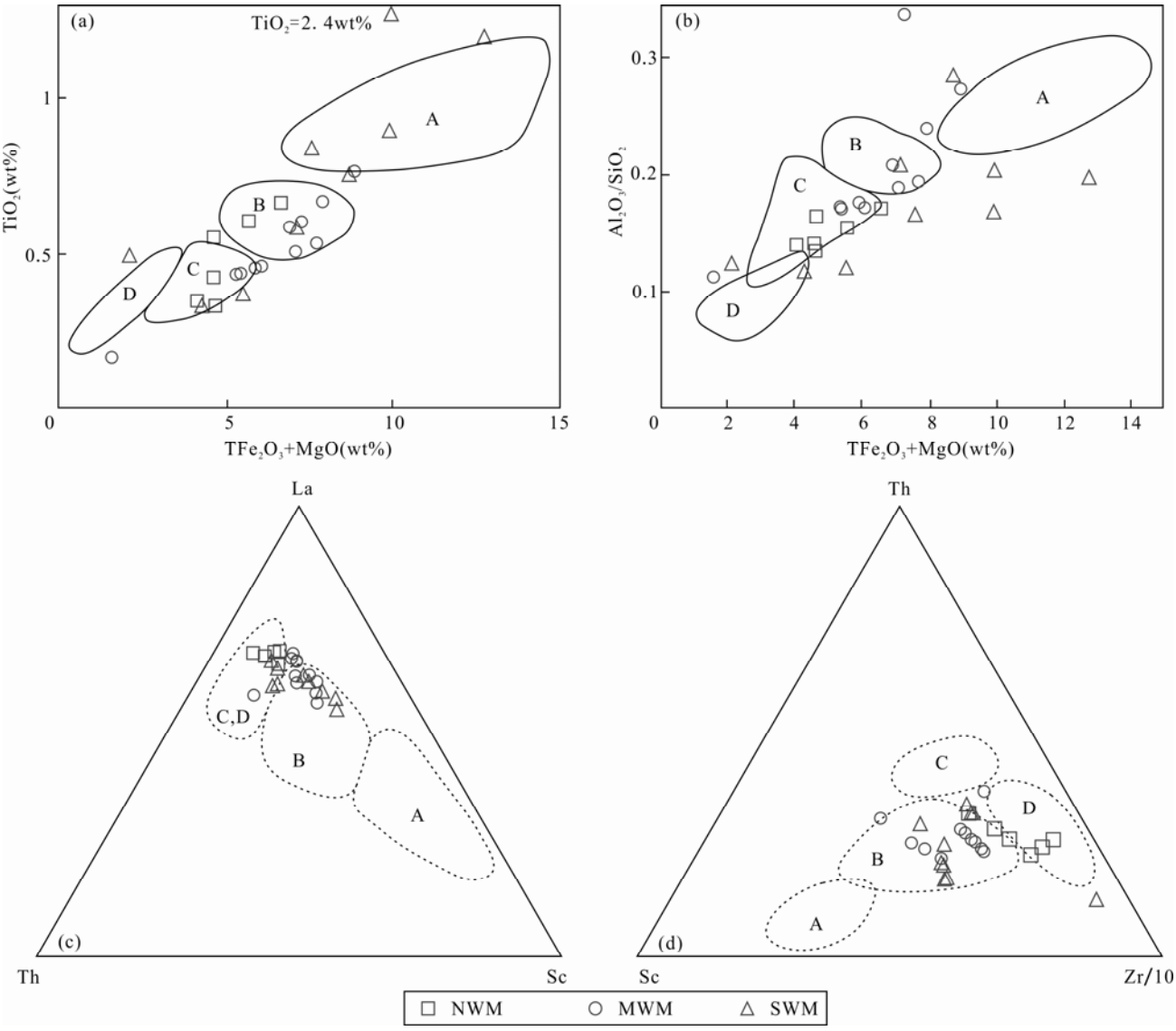

Fig. 10. Major element (a, b, after Bhatia, 1983) and trace element (c, d, after Bhatia and Crook, 1986) tectonic setting discrimination diagrams for Upper Triassic sandstones.
A = oceanic island arc; B = continental island arc; C = active continental margin; D = passive margin.

Mianlue Ocean led to collision between the South China and North China blocks and formation of the Qinling Orogenic Belt (Dong and Santosh, 2016). During this period, a large volume of arc-related, syn- and post-collisional magmatic rocks were generated. The plotting of the MWM and SWM samples also suggest their provenance were Qinling-Qilian Orogenic Belt, and therefore show the continental island arc setting of the parent rocks. However, the plotting of samples in the NWM is not consistent with the petrography and the regional tectonic background. Sedimentary system, tectonic features and geochemical characteristics of Rujigou basalt all indicate the tectonic setting of NWM is a rift basin in extension environment (Ritts et al., 2004; Wang et al., 2005; Liu et al., 2006; Yang et al., 2010). We interpret this "paradox" as a consequence of recycling. Previous researches show the NWM and adjacent regions experienced complex oceanic-continental evolution process during the Paleozoic (Zhang et al., 2011, 2015; Xu et al., 2015), including subduction, consumption, final closure of the oceanic crust and the sequence collisional orogeny. As mentioned above, the northwest sediments have a typical recycled nature. Thus, the sediments exhibit inherited geochemical features of the complex tectonic settings.

5.3.2 Proto-boundary of the western Ordos Basin

It is one of the important questions in science theory and production practice in western Ordos Basin to determine the proto-basin boundary in the Late Triassic. Based on the analysis of petrography, geochemistry and sedimentology, together with previously published literature, we try to discuss the Late Triassic boundary of the western Ordos Basin.

To the west, we believe the boundary of proto-basin of Ordos Basin went across Liupanshan area and extended to HCB. The evidences are described here. Firstly, the palaeocurrent direction in HCB was eastward, the same as that in western margin of the Ordos Basin (Fig. 1b). And sedimentary facies of sandstones support that the HCB connected with Ordos Basin during the Late Triassic, and belonged to distal portion of fluvial-delta system (Bai et al., 2006; Zhao et al., 2006). Secondly, the similar heavy mineral assemblage (garnet-zircon) and REE distribution patterns (Fig. 5) between HCB and Ordos Basin could also provide significant evidence that they were both developed in the same sedimentary system (e.g., Zhao et al., 2006; Yang et al., 2011). Thirdly, paleontological characteristic suggests that the fossil assemblage developed in the Upper Triassic from HCB, which belongs to *Danaeopsis-Bernoullia* formation, is similar with that from Ordos Basin (BGMRNHAR, 1990). Finally, the SHRIMP U-Pb zircon age of tuff at the bottom of the Upper Triassic Nanying'er Group in Baojishan (244.1±3.8 Ma) and Wangjiashan (244.9±2.8 Ma), are comparable with that of Yanchang Formation within the Ordos Basin (239.7±1.7–241.3±2.4 Ma; Xin et al., 2013a, b). To the northwest, the Upper Triassic in Shigouyi area are composed of medium-grained sandstone and fine conglomerate, with groove bedding, cross-bedding and parallel bedding, which is obviously not consistent with piedmont or turbid deposit (Zhao et al., 2006). Futhermore, heavy mineral assemblage showed similar combination in Rujigou-Shigouyi-Dingbian area, with stable mineral increasing from northwest to southeast (Liu, 2009). These characteristics reflect that the Shigouyi was not the northwestern boundary of Ordos Basin during the Late Triassic, while the Helanshan area is (Bai et al., 2006; Zhao et al., 2006). To the southwest, the sedimentary system in Kongtongshan is typical alluvial deposits. From southwest to northeast, the grain size and layer thickness decreased. In Qingyang-Huachi area within basin, the layer thickness gradually stabilized, lithology is characterized by fine clastic rocks, lacustrine turbidite sand bodies and source rocks developed (Fu et al., 2005). The characteristics of these sedimentology and lithofacies indicate that the Kongtongshan area is the southwestern boundary of the Ordos Basin in the Late Triassic period.

6 Conclusions

A combination of petrography, geochemistry and sedimentology analysis provides new insights to discuss the provenance and tectonic implications of the Upper Triassic sandstones from the western Ordos Basin, NW China, and the following conclusions were drawn:

(1) CIA and CIW values suggest the sediments come from different chemical weathering sources. Most samples come from weak weathering source area, while a few samples from MWM and SWM fall in the intermediate weathering area.

(2) Based on petrology, geochemistry and palaeocurrent evidence, we conclude that the provenance of NWM was mainly from the Alxa Block with a typical recycling nature, while the provenance of MWM and SWM were mainly from the Qinling-Qilian Orogenic Belt.

(3) Multiple discrimination diagrams suggest that the parent rocks of the MWM and SWM sandstones were mainly derived from continental island arc, while the NWM samples show a complex nature. These features are related with the Qinling-Qilian Orogenic Belt as provenance and recycled ancient sediments, respectively.

(4) Based on the analysis of petrography, geochemistry, sedimentology and previous researches, we believe that the Kongtongshan area and Helanshan area were the southwestern and northwestern boundary of the Ordos Basin in the Late Triassic period, respectively. However, there is no clear boundary between HCB and Ordos Basin, i.e., the western boundary got across Liupanshan area.

Acknowledgements

This work is granted by the National Natural Science Foundation of China [Grant No. 41802119 and 41602212], Natural Science Foundation of Shaanxi [Grant No. 2019JQ-088], Special Projects of China Geological Survey [Grant No. 12120113039900 and 12120114009201], and Doctor's fund of Xi'an University of Science and Technology [Grant No. 2017QDJ051].

Manuscript received Sept. 28, 2018

accepted Dec. 20, 2018
associate EIC XIAO Yitan
edited by LIU Lian

References

Aubert, D., Stille, P., and Probst, A., 2001. REE fractionation during granite weathering and removal by waters and suspended loads: Sr and Nd isotopic evidence. Geochemica et Cosmochimica Acta, 65(3): 387–406.

Bai, Y.L, Wang, X.M., Liu, H.Q., and Li, T.S., 2006. Determination of the borderline of the western Ordos basin and its geodynamics background. Acta Geologica Sinica, 80 (6): 792–813 (in Chinese with English abstract).

Bao, C., Chen, Y.L., Li, D.P., and Wang, S.H., 2014. Provenances of the Mesozoic sediments in the Ordos Basin and implications for collision between the North China Craton (NCC) and the South China Craton (SCC). Journal of Asian Earth Sciences, 96: 296–307.

BGMRGP (Bureau of Geology and Mineral Resources of Gansu Province), 1989. Regional Geology of Gansu Province. Beijing: Geological Publishing House, 1–692 (in Chinese)

BGMRNHAR (Bureau of Geological Mineral Resources of Ningxia Hui Autonomous Region), 1990. Regional Geology of Ningxia Hui Autonomous Region. Beijing: Geological Publishing House, 443 (in Chinese).

Bhatia, M.R., 1983. Plate tectonics and geochemical composition of sandstones. The Journal of Geology, 91: 611–627.

Bhatia, M.R., and Crook, K.A.W., 1986. Trace element characteristics of graywackes and tectonic setting discrimination of sedimentary basins. Contributions to Mineralogy and Petrology, 92: 181–193.

Bruguier, O., Lancelot, J.R., and Malavieille, J., 1997. U-Pb dating on single detrital zircon grains from the Triassic Songpan-Ganze Flysch (Central China): provenance and tectonic correlations. Earth and Planetary Science Letters, 152 (1–4): 217–231.

Cox, R., Lowe, D.R., and Cullers, R.L., 1995. The influence of sediment recycling and basement composition on evolution of mudrock chemistry in south western United States. Geochimica Et Cosmochimica Acta, 59(14): 2919–2940.

Cullers, R.L., 1994 The controls on the major and trace element variation of shales, siltstones, and sandstones of Pennsylvanian-Permian age from uplifted continental blocks in Colorado to platform sediment in Kansas, USA. Geochimica et Cosmochimica Acta, 58(22): 4955–4972

Cullers, R.L., 2000. The geochemistry of shales, siltstones and sandstones of Pennsylvanian-Permian age, Colorado, USA: Implications for provenance and metamorphic studies. Lithos, (3), 51: 181–203.

Cullers, R.L., and Podkovyrov, V.N., 2000. Geochemistry of the Mesoproterozoic Lakhanda shales in southeastern Yakutia, Russia: implications for mineralogical and provenance control and recycling. Precambrian Research, 104(1–2): 77–93.

Cullers, R.L., and Podkovyrov, V.N., 2002. The source and origin of terrigenous sedimentary rocks in the Mesoproterozoic Ui Group, south-eastern Russia. Precambrian Research, 117: 157–183.

DeCelles, P.G., Langford, R.P., and Schwartz, R.K., 1983. Two new methods of paleocurrent determination from trough cross -stratification. Journal of Sedimentary Petrology, 53: 629–642.

Diskin, S., Evans, J., Fowler, M.B., and Guion, P.D., 2011. Recognising different sediment provenances within a passive continental margin setting: towards characterizing a sediment source to the west of the British late Carboniferous sedimentary basins. Chemical Geology, 283(3–4): 143–160.

Dong, Y.P., and Santosh, M., 2016. Tectonic architecture and multiple orogeny of the Qinling Orogenic Belt, Central China. Gondwana Research, 29(1): 1–40.

Duan, Y., 2012. Geochemical characteristics of crude oil in fluvial deposits from Maling oilfield of Ordos Basin, China. Organic Geochemistry, 52: 35–43.

Floyd, P.A., and Leveridge, B.E., 1987. Tectonic environment of the Devonian Gramscatho Basin, South Cornwall: Framework mode and geochemical evidence from turbiditic sandstones. Journal of Geology Society London, 144: 531–542.

Fu, J.H, Guo, Z.Q., and Deng, X.Q., 2005. Sedimentary facies of the Yanchang Formation of Upper Triassic and petroleum geological implication in southwestern Ordos Basin. Journal of Palaeogeography, 7(1): 34–44 (in Chinese with English abstract).

Geng, Y.S., Wang, X.S., Shen, Q.H., and Wu, C.M., 2006. Redefinition of the Alxa Group-complex (Precambrian metamorphic basement) in the Alxa area, Inner Mongolia. Geology in China, 33(1): 138–145 (in Chinese with English abstract).

Geng, Y.S., Wang, X.S., Shen, Q.H., and Wu, C.M., 2007. Chronology of the Precambrian metamorphic series the Alxa area, Inner Mongolia. Geology in China, 34(2): 251–261 (in Chinese with English abstract).

Harnois, L., 1988. The CIW index: a new chemical index of weathering. Sedimentary Geology, 55(3–4): 319–322.

Holland, H.D., 1978. The chemistry of the atmosphere and the oceans. New York: John Wiley and Sons Inc., 351.

Kassi, A.M., Grigsby, J.D., Khan, A.S., and Kasi, A.K., 2015. Sandstone petrology and geochemistry of the Oligocene-Early Miocene Panjgur Formation, Makran accretionary wedge, southwest Pakistan: Implications for provenance, weathering and tectonic setting. Journal of Asian Earth Sciences, 105: 192 –207.

Kröner, A., Zhang, G.W., and Sun, Y., 1993. Granulites in the Tongbai Area, Qinling Belt, China: geochemistry, petrology, single zircon geochronology, and implications for the tectonic evolution of eastern Asia. Tectonics, 12(1): 245–255.

Lewin, A., Meihold, G., Hinderer, M., Dawit, E.L., and Bussert, R., 2018. Provenance of sandstones in Ethiopia during Late Ordovician and Carboniferous–Permian Gondwana glaciations: Petrography and geochemistry of the Enticho Sandstone and the Edaga Arbi Glacials. Sedimentary Geology, 375: 188–202.

Li, B., 2006. Analysis for depositional facies, palecurrent and provenance of the Chang 8 and Chang 6 member in Xifeng-Heshui region, Ordos Basin. Xi'an: Northwest University (Ph. D thesis).

Li, J.J., Shen, B.F., and Li, H.M., Zhou, H.Y., Guo, L.J., and Li, C.Y., 2004a. Single zircon U-Pb age of granodioritic gneiss in the Bayan Ul area, western Inner Mongolia. Geological Bulletin of China, 23(12): 1243–1245 (in Chinese with English abstract).

Li, X.H., Su, L., Song, B., and Liu, D.Y., 2004b. SHRIMP U-Pb zircon age of the Jinchuan ultramafic intrusion and its geological significance. Chinese Science Bulletin, 49(4): 420–422.

Li, X.B., Liu, X.Y., Zhou, S.X. Liu, H.Q., Chen, Q.L., Wang, J., Liao, J.B., and Huang, J.P, 2012. Hydrocarbon origin and reservoir forming model of the Lower Yanchang Formation, Ordos Basin. Petroleum Exploration and Development, 39(2): 184–193.

Liao, C.Z., Zhang, Y.Q., and Wen, C.S., 2007. Structural styles of the eastern boundary zone of the Ordos Basin and its regional tectonic significance. Acta Geologica Sinica, 81(4): 466–474 (in Chinese with English abstract).

Liu, S.F., Ke, A.R., Wu, L.Y., and Huang, S.J., 1997. Sediment provenance analysis and its tectonic significance in the foreland basin of the Ordos southwestern margin. Acta Sedimentologica Sinica, 15(1): 156–160 (in Chinese with English abstract).

Liu, S.F., and Yang, S.G., 1997. The differences between the southwestern and the northwestern Ordos Basin and their forming mechanism. Scientia Geologica Sinica, 32(3): 397–408 (in Chinese with English abstract).

Liu, S.F., 1998. The coupling mechanism of basin and orogen in the western Ordos Basin and adjacent regions of China. Journal of Asian Earth Sciences, 16(4): 369–383.

Liu, S. F. and Yang, S. G., 2000. Upper Triassic-Jurassic sequence stratigraphy and its structural controls in the western Ordos Basin, China. Basin Research, 12(1): 1–18.

Liu, C.Y., Zhao, H.G., Wang, F., and Chen, H., 2005. Attributes of the Mesozoic structure on the west margin of the Ordos

Basin. Acta Geologica Sinica, 79(6): 737–747 (in Chinese with English abstract).
Liu, C.Y., Zhao, H.G., Gui, X.J., Yue, L.P., Zhao, J.F., and Wang, J.Q., 2006. Space-Time Coordinate of the Evolution and Reformation and Mineralization Response in Ordos Basin. Acta Geologica Sinica, 80(5): 617–638 (in Chinese with English abstract).
Liu, Y., Liu, X.M., Hu, Z.C., Diwu, C.R., Yuan, H.L., and Gao, S., 2007 Evaluation of accuracy and long-term stability of determination of 37 trace elements in geological samples by ICP-MS. Acta Petrologica Sinica, 23(5): 1203–1210 (in Chinese with English abstract).
Liu, C., 2009. Restoration of the Yanchang period Late Triassic basin in the southwestern margin of Ordos Basin. Xi'an: Northwest University (Ph. D thesis) (in Chinese with English abstract).
Liu, H.W., Wang, J., Liu, Q.M., and Zhao, X., 2012. Favorable reservoir distribution and its controlling factors of the Chang 8 interval of Upper Triassic Yanchang Formation in Jiyuan Area, Ordos Basin. Journal of Palaeogeography, 14(3): 285–294 (in Chinese with English abstract).
Liu, G.D., Yang, W.W., Feng, Y., Ma, H.Y., and Du, Y.G, 2013. Geochemical characteristics and genetic types of crude oil from Yanchang Formation in Longdong Area, Ordos Basin. Earth Science Frontiers, 20(2): 108–115 (in Chinese with English abstract).
McLennan, S.M., Taylor, S.R., and Kröner, A. 1983. Geochemical evolution of Archean shales from South Africa I. The Swaziland and Pongola Supergroups. Precambrian Research, 22(1–2): 93–124.
McLennan, S.M., Hemming, S., McDaniel, D.K., and Hanson, G.N., 1993. Geochemical approaches to sedimentation, provenance, and tectonics. Special Paper of the Geological Society of America, 284: 21–40.
McLennan, S.M., 2001. Relationships between the trace element composition of sedimentary rocks and upper continental crust. Geochemistry Geophysics Geosystems, 2(4): 1021–1024.
Nesbitt, H.W., and Young, G.M., 1982. Early Proterozoic climates and plate motions inferred from major element chemistry of lutites. Nature, 299(5885): 715–717.
Nesbitt, H.W., and Young, G.M., 1984. Prediction of some weathering trends of plutonic and volcanic rocks based on thermodynamic and kinetic considerations. Geochimica et Cosmochimica Acta, 48(7): 1523–1534.
Nesbitt, H.W., and Young, G.M., 1989. Formation and diagenesis of weathering profiles. The Journal of Geology, 97 (2): 129–147.
Nyakairu, G.W.A., and Koeberl, V., 2001. Mineralogical and chemical composition and distribution of rare earth elements in clay-rich sediments from central Uganda. Geochemical Journal, 35: 13–28.
Patterson, J.H., Ramsden, A.R., Dale, L.S., and Fardy, J.J., 1986. Geochemistry and mineralogical residences of trace elements in oil shales from Julia Creek, Queensland, Australia. Chemical Geology, 55(1–2): 1–16.
Ritts, D.R., Hanson, A.D., Darby, B.J., Nanson, L., and Berry, A., 2004. Sedimentary record of Triassic intraplate extension in North China: evidence from the nonmarine NW Ordos Basin, Helan Shan and Zhuozi Shan. Tectonophysics, 386(3): 177–202.
Ritts, B.D., Weislogel, A., Graham, S.A., and Darby, B.J., 2009. Mesozoic tectonics and sedimentation of the giant polyphase nonmarine intraplate Ordos Basin, Western North China Block. International Geology Review, 51(2): 95–115.
Roser, B.P., and Korsch, R.J., 1986. Determination of tectonic setting of sandstone-mudstone suites using SiO_2 content and K_2O/Na_2O ratio. The Journal of Geology, 94: 635–650.
Roser, B.P., and Korsch, R.J., 1988. Provenance signatures of sandstone-mudstone suites determined using discriminant function analysis of major-element data. Chemical Geology, 67(1–2): 119–139.
Saminpanya, S., Duangkrayom, J., Jintasakul, P., and Hanta, R., 2014. Petrography, mineralogy and geochemistry of Cretaceous sediments samples from western Khorat Plateau, Thailand, and considerations on their provenance. Journal of Asian Earth Sciences, 83(2): 13–34.
Shaw, D.M., 1968. A review of K-Rb fractionation trends by covariance analysis. Geochimica et Cosmochimica Acta, 32 (6): 573–602.
Shi, G.Z., Wang, H., Huang, C.Y., Yang, S.Y., and Song, G.Z., 2016. Provenance and tectonic setting of middle-upper Devonian sandstones in the Qinling Orogen (Shanyang area): New insights from geochemistry, heavy minerals and tourmaline chemistry. Tectonophysics, 688: 11–25.
Song, S.G., Niu, Y.L., Su, L., and Xia, X.H., 2013. Tectonics of the north Qilian orogen, NW China. Gondwana Research, 23 (4): 1378–1401.
Stephen, J.V., and Mark, B.A., 1999. Evolution of the Minle and Chaoshui Basins, China: Implications for Mesozoie strike-slip basin formation in Central Asia, Geological Society of America Bulletin, 111(5): 725–742.
Sun, S.S., and McDonough, W.F., 1989 Chemical and isotopic systematic of oceanic basalts: implications for mantle composition and process. Geological Society Special Publication, 42(1): 313–345.
Sun, Z., Xie, Q., and Yang, J., 1989. Ordos basin-a typical example of an unstable cratonic interior superimposed basin. In Chinese Sedimentary Basins (ed X. Zhu), New York: Elsevier, 63–75.
Tang, X.Y., Guo, Z.M., and Chen, H.L., 1992. The study and petroleum prospect of Thrust Nappe in the West margin of Shanxi-Gansu-Ningxia Basin. Xi'an: Northwest University Press (in Chinese).
Taylor, S.R., and McLennan, S.M., 1985. The continental crust: Its composition and evolution, an examination of the geochemical record preserved in sedimentary rocks. Oxford: Blackwell Scientific Publications.
Tung, K.A., Yang, H.Y., and Liu, D.Y., 2007a. SHRIMP U-Pb geochronology of detrital zircons from the Longshoushan Group and its tectonic significance. Chinese Science Bulletin, 52(6): 1414–1425.
Tung, K.A., Yang, H.J., Yang, H.Y., Liu, D.Y., Zhang, J.X., Wan, Y.S., and Tseng, C.Y., 2007b. SHRIMP U-Pb geochronology of the zircons from the Precambrian basement of the Qilian Block and its geological significances. Chinese Science Bulletin, 52: 2687–2701.
Wang, F., Liu, C.Y., Yang, X.K., and Su, Q.C., 2005. Geologic geochemical features of basalt in Ruqi clough of Helan mountain and its structural environmental significance. Petroleum Geology and Oilfield Development in Daqing, 24 (4): 25–27 (in Chinese with English abstract).
Wang, X.Z., Gao, S.L., and Gao, C., 2014. Geological features of Mesozoic lacustrine shale gas in south of Ordos Basin, NW China. Petroleum Exploration and Development, 41(3): 326–337.
Wang, F.F., Liu, C.Y., Niu, H.Q., Zhou, N.C., Li, X.H., Luo, W., Zhang, D.D., and Zhao, Y., 2018. In-situ chemical age of the sandstone-hosted uranium deposit in Ningdong Area on the western margin of the Ordos Basin, North China. Acta Geologica Sinica (English Edition), 92(1): 406–407.
Wu, S.T., Zou, C.F., Zhu, R.K., Yao, J.L., Tao, S.Z., Yang, Z., Zhai, X.F., Cui, J.W., and Lin, S.H., 2018. Characteristics and origin of tight oil accumulations in the Upper Triassic Yanchang Formation of the Ordos Basin, North-Central China. Acta Geologica Sinica (English Edition), 90(5): 1821–1837.
Waston, M.P., Hayward, A.B., Parkinson, D.N., and Zhang, Z.M., 1987. Plate tectonic history, basin development and petroleum source rock deposition onshore China. Marine and Petroleum Geology, 4(3): 205–225.
Whitmore, G.P., Crook, K.A., and Johnson, D. P., 2004 Grain size control of mineralogy and geochemistry in modern river sediment, New Guinea collision, Papua New Guinea. Sedimentary Geology, 171(1–4): 129–157
Wronkiewicz, D.J., and Condie, K.C., 1987. Geochemistry of Archean shales from the Witwatersrand Supergroup South Africa: source-area weathering and provenance. Geochim. Geochimica et Cosmochimica Acta, 51(9): 2401–2416.
Wronkiewicz, D.J., and Condie, K.C., 1990. Geochemistry and mineralogy of sediments from the Ventersdorp and Transvaal

Supergroups, South Africa: cratonic evolution during the early Proterozoic. Geochimica et Cosmochimica Acta, 54: 343–354.
Xie, X.Y., and Heller, P.L., 2013. U-Pb detrital zircon geochronology and its implications: the early Late Triassic Yanchang Formation, south Ordos Basin, China. Journal of Asian Earth Sciences, 64: 86–98.
Xie, X.Y., 2016. Provenance and sediment dispersal of the Triassic Yanchang Formation, southwest Ordos Basin, China, and its implication. Sedimentary Geology, 335: 1–16.
Xin, B.S., Yang, H., Fu, J.H., Wang, D.Y., Yao, J.L., Zhang, Y., and Zuo, B., 2013a. SHRIMP U-Pb zircon age and its stratigraphic significance of tuff at the bottom of the Upper Triassic Nanying'er Group, Mount Baoji Area, Jingyuan County, Gansu Province. Geological Review, 59(2): 267–273 (in Chinese with English abstract).
Xin, B.S., Yang, H., Wang, D.Y., Fu, J.H., Yao, J.L., Luo, A.X., and Zhang, Y., 2013b. SHRIMP U-Pb zircon age and its stratigraphic significance of tuff at the Wangjiashan area, Jingyuan County, Gansu Province. Advances in Earth Science, 28(9): 1043–1048 (in Chinese with English abstract).
Xiu, Q.Y., Yu, H.F., Li, Q., Zuo, G.C., Li, J.W., and Cao, C.J., 2004. Discussion on the petrogenic time of Longshoushan Group, Gansu Province. Acta Geologica Sinica, 78(3): 366–373 (in Chinese with English abstract).
Xu, S.M., Feng, H.W., Li, S.Z., Li, M., Somerville, I., Bi, H.M., and Ji, Y., 2015. Closure time in the east Qilian Ocean and early Paleozoic Ocean-continent configuration in the Helan Mountains and adjacent regions, NW China. Journal of Asian Earth Sciences, 113: 575–588.
Yang, Z., Cheng, Y., and Wang, H., 1986. The Geology of China. Oxford Monographs on Geology and Geophysics No.3. Clarendon Press, Oxford (303 pp.).
Yang, H., Fu, J.H., Ouyang, Z.J., Sun, L.Y., and Ma, Z.R., 2010. U-Pb Zircon dating of the Daling-Gugutai basalt in Rujigou on the western Margin of Ordos Basin. Acta Geoscientica Sinica, 31(2): 229–236 (in Chinese with English abstract).
Yang, H., Fu, J.H., Ouyang, Z.J., and Sun, L.Y., 2011. Analysis of tectonic-sedimentory setting in middle and upper Triassic in the west margin of the Ordos Basin. Acta Sedimentologica Sinica, 29(3): 427–439 (in Chinese with English abstract).
Yang, J.J., 1990. The basic characteristics of the western Ordos thrust belt. In Structure and Oil-Gas of the Thrust Belt in the Western Ordos Basin (eds J. J. Yang), Gansu Scientific and Technological Publishing House, 91–105 (in Chinese).
Yang, Y., Li, W., and Ma, L., 2005. Tectonic and stratigraphic controls of hydrocarbon systems in the Ordos Basin: a multicycle cratonic basin in Central China. AAPG Bulletin, 89 (2): 255–269.
Yin, A., and Nie, S., 1996. A phanerozoic palinspastic reconstruction of China and its neighboring regions. In Tectonic Evolution of Asia (eds A. Yin and T. M. Harrison). Cambridge: Cambridge University Press, 442–485.
Zhang, G.W., Xiang, L., and Meng, Q.R., 1995. The Qinling Orogen and intracontinental orogen mechanisms. Episodes, 18: 36–39.
Zhang, J., 2002. A study on the structures and evolution of the juncture area of Shanxi, Gansu province and Ningxia Autonomous Region since Paleozoic time. Beijing: Institute of Geology, Seismological Bureau of China. (Ph. D thesis) (in Chinese with English abstract).
Zhang, J.L., and Zhang, X., 2007 Element geochemistry of sandstones in the Silurian of central Tarim basin and the significance in provenance discrimination. Acta Petrologica Sinica, 23(11) 2990–3002 (in Chinese with English abstract).
Zhang, J., Li, J.Y., Liu, J.F., and Feng, Q.W., 2011. Detrital zircon U-Pb ages of middle Ordovician flysch sandstones in the western ordos margin: new constraints on their provenances, and tectonic implications. Journal of Asian Earth Sciences, 42(5): 1030–1047.
Zhang, J., Zhang, Y.P., Xiao, W.X., Wang, Y.N., and Zhang, B.H., 2015. Linking the Alxa terrane to the eastern Gondwana during the early Paleozoic: constraints from detrital zircon U-Pb ages and Cambrian sedimentary records. Gondwana Research, 28(3): 1168–1182.
Zhao, W.Z., Wang, X.M., Guo, Y.R., Liu, H.Q., and Bai, Y.L., 2006. Restoration and tectonic reworking of the Late Triassic basin in western Ordos Basin. Petroleum Exploration and Development, 33(1): 6–13 (in Chinese with English abstract).
Zhao, X.C., Liu, C.Y., Wang, J.Q., Zhao, Y., Zhang, D.D., Wang, L., Deng, Y., and Guo, P., 2016. Mesozoic-Cenozoic tectonic uplift events of Xiangshan Mountain in northern North-South Tectonic Belt, China. Acta Petrologica Sinica, 32 (7): 2124–2136 (in Chinese with English abstract).
Zhao, Y., Liu, C.Y., Niu, H.Q., Zhao, X.C., Zhang, D.D., Yang, D., and Deng, H., 2017.Trace and rare earth element geochemistry of crude oils and their coexisting water from the Jiyuan Area of the Ordos Basin, N China. Geological Journal, 53(6): 336–348.

About the first author

ZHAO Xiaochen, male, born in 1989 in Xianyang City, Shaanxi Province; doctor; graduated from Northwest University; lecturer, College of Geology and Environment, Xi'an University of Science and Technology. He is now interested in the study on basin analysis. E-mail address: zxcnwu@126.com.

About the corresponding author

LIU Chiyang, male, born in 1953 in Xi'an City, Shaanxi Province; master; professor, Department of Geology, Northwest University. He is now interested in the study on the sedimentary basin analysis and dynamics, and post-reconstruction and restoration of original basins. Email: lcy@nwu.edu.cn; phone: 029-88302202.